The Geological Society of America
Special Paper 522

Iron mineralogy and redox conditions during deposition of the mid-Proterozoic Appekunny Formation, Belt Supergroup, Glacier National Park

Sarah P. Slotznick*
Division of Geological and Planetary Sciences, California Institute of Technology, 1200 East California Boulevard, Pasadena, California 91125, USA

Don Winston†
Department of Geosciences, University of Montana, Missoula, Montana 59812, USA

Samuel M. Webb
Stanford Synchrotron Radiation Lightsource, Menlo Park, California 94025, USA

Joseph L. Kirschvink
Division of Geological and Planetary Sciences, California Institute of Technology, 1200 East California Boulevard, Pasadena, California 91125, USA, and *Earth-Life Science Institute, Tokyo Institute of Technology, Meguro-ku, Toyko 152-8550, Japan*

Woodward W. Fischer
Division of Geological and Planetary Sciences, California Institute of Technology, 1200 East California Boulevard, Pasadena, California 91125, USA

ABSTRACT

The redox state of the mid-Proterozoic oceans, lakes, and atmospheres is still debated, but it is vital for understanding the emergence and rise of macroscopic organisms and eukaryotes. The Appekunny Formation, Belt Supergroup, Montana, contains some of these early macrofossils dated between 1.47 Ga and 1.40 Ga and provides a well-preserved record of paleoenvironmental conditions. We analyzed the iron chemistry and mineralogy in samples from Glacier National Park, Montana, by pairing bulk rock magnetic techniques with textural techniques, including light microscopy, scanning electron microscopy, and synchrotron-based X-ray absorption spectroscopy. Field observations of the Appekunny Formation combined with mineralogical information allowed revised correlations of stratigraphic members across the park. However, late diagenetic and/or metasomatic fluids affected primary iron phases, as evidenced by prevalent postdepositional phases including base-metal sulfides. On the west side of the park, pyrrhotite and chlorite rims formed during burial

*sslotz@caltech.edu
†retired

Slotznick, S.P., Winston, D., Webb, S.W., Kirschvink, J.L., and Fischer, W.W., 2016, Iron mineralogy and redox conditions during deposition of the mid-Proterozoic Appekunny Formation, Belt Supergroup, Glacier National Park, *in* MacLean, J.S., and Sears, J.W., eds., Belt Basin: Window to Mesoproterozoic Earth: Geological Society of America Special Paper 522, p. 221–242, doi:10.1130/2016.2522(09).

metamorphism in at least two recrystallization events. These complex postdepositional transformations could affect bulk proxies for paleoredox. By pairing bulk and textural techniques, we show primary records of redox chemistry were preserved in early diagenetic and often recrystallized framboidal pyrite, submicron magnetite grains interpreted to be detrital in origin, and red-bed laminae interpreted to record primary detrital oxides. Based on these observations, we hypothesize that the shallow waters of the mid-Proterozoic Belt Basin were similar to those in modern marine and lacustrine waters: fully oxygenated, with detrital reactive iron fluxes that mineralized pyrite during organic diagenesis in suboxic, anoxic, and sulfidic conditions in sedimentary pore waters.

INTRODUCTION

Currently exposed across parts of Montana, Idaho, and Washington, United States, and Alberta and British Columbia, Canada, the Belt Supergroup is one of the best-preserved and extensive mid-Proterozoic sedimentary terranes (Fig. 1A). This thick sedimentary succession was deposited between 1470 Ma and 1401 Ma (Anderson and Davis, 1995; Evans et al., 2000; Sears et al., 1998) and provides an important paleontological perspective on the evolution of eukaryotes and multicellularity (Knoll et al., 2006). The Belt Supergroup is well known for its stromatolites, but it also contains a diversity of other microfossils and macrofossils (Horodyski et al., 1989). In the mudstones of its lower portion, two macrofossils have been studied in great detail. First identified by Charles Doolittle Walcott (1899) in the Greyson Shale and later renamed (Walter et al., 1976), *Grypania spiralis* is a curved or coiled ribbon, 0.2–1.7 mm wide, and 6–14 mm in coiled diameter, and it has been nonuniquely interpreted as eukaryotic algae as well as a consortia of several microscopic organisms (Horodyski et al., 1989; Knoll et al., 2006; Walter et al., 1976). Within the stratigraphically correlated Appekunny Formation, *Horodyskia moniliformi*s has the general appearance of a string of beads with diameters of 2.1–9.2 mm and lengths up to 15 cm, and it has been interpreted to represent a wide range of different organisms, including algae (Grey and Williams, 1990; Horodyski, 1993), prokaryotic colonies (Knoll et al., 2006), tissue-grade colonial eukaryotes (Fedonkin and Yochelson, 2002), sponges (Hofmann, 2001), foraminifers (Dong et al., 2008), and lichen (Retallack et al., 2013). No matter their affinity, understanding more about the environmental conditions where these early macroscopic organisms lived will tell us more about the pacing of evolution and how it might have been aided, frustrated, or unaffected by changing environmental conditions.

Major first-order questions exist concerning the redox status of the oceans, lakes, and atmosphere during mid-Proterozoic time. Based broadly on a gap in the preserved record of banded iron formation, red beds, marine manganese deposits, and the conspicuous presence of carbonate platforms, it has been suggested that the mid-Proterozoic subaqueous basins were oxygenated at (nearly) all depths (Cloud, 1968; Holland, 1984, 2006; Slack et al., 2007). Based on theory and sulfur isotope records, others have suggested that if atmospheric oxygen values were lower than today with similar levels of marine primary production, then the deep oceans would have been anoxic and sulfidic (i.e., euxinic), with the consequence that the lack of banded iron formations was due to an increase in water-column sulfide leading to iron-sulfide precipitation (Canfield, 1998). Recently, bulk geochemical techniques have queried the composition and redox state of mid-Proterozoic basins using the sequential extraction technique known as iron speciation as well as trace-metal work (e.g., Gilleaudeau and Kah, 2015; Kendall et al., 2009; Planavsky et al., 2011; Shen et al., 2003; Sperling et al., 2014). Iron speciation data suggest anoxic, euxinic, and oxic waters varying between different basins, different water depths, and temporally, with dominant anoxic and sulfur-poor (i.e., ferruginous) conditions despite the lack of iron formation deposition (Poulton and Canfield, 2011; Sperling et al., 2015). This new notion of a ferruginous Proterozoic world based on iron speciation is distinctly different from the aforementioned canonical views of mid-Proterozoic paleoenvironments.

Several geochemical studies have focused specifically on the paleoredox state and geochemistry of the Belt Basin during deposition of the Belt Supergroup. Arguments for a stratified euxinic basin during deposition of the lower Belt Supergroup were made on the basis of sulfate levels and sulfur isotopes (Gellatly and Lyons, 2005; Luepke and Lyons, 2001; Lyons et al., 2000) as well as presence of basinwide sedimentary laminations similar to those found in the Black Sea (Huebschman, 1973; Lyons et al., 2000). Bottom water suboxic to euxinic conditions were also inferred from the high (several weight percent) organic content observed in shales regionally (Lyons et al., 2000) and the conspicuous syndepositional to early diagenetic sulfide and base metal deposits of Pb, Cu, and Zn (Graham et al., 2012; Hamilton et al., 1982; Huebschman, 1973; Slotznick et al., 2015). However, iron speciation results on the same samples suggested instead anoxic and ferruginous conditions for the water column during deposition of the lower Belt Supergroup (Planavsky et al., 2011). Additionally, recent nitrogen isotope studies suggested oxygenated surface waters (Stüeken, 2013). Importantly, most of these studies focused on samples from the Helena Embayment, which is distinct from, but stratigraphically correlated to, the units in Glacier National Park and the rest of the Belt Basin.

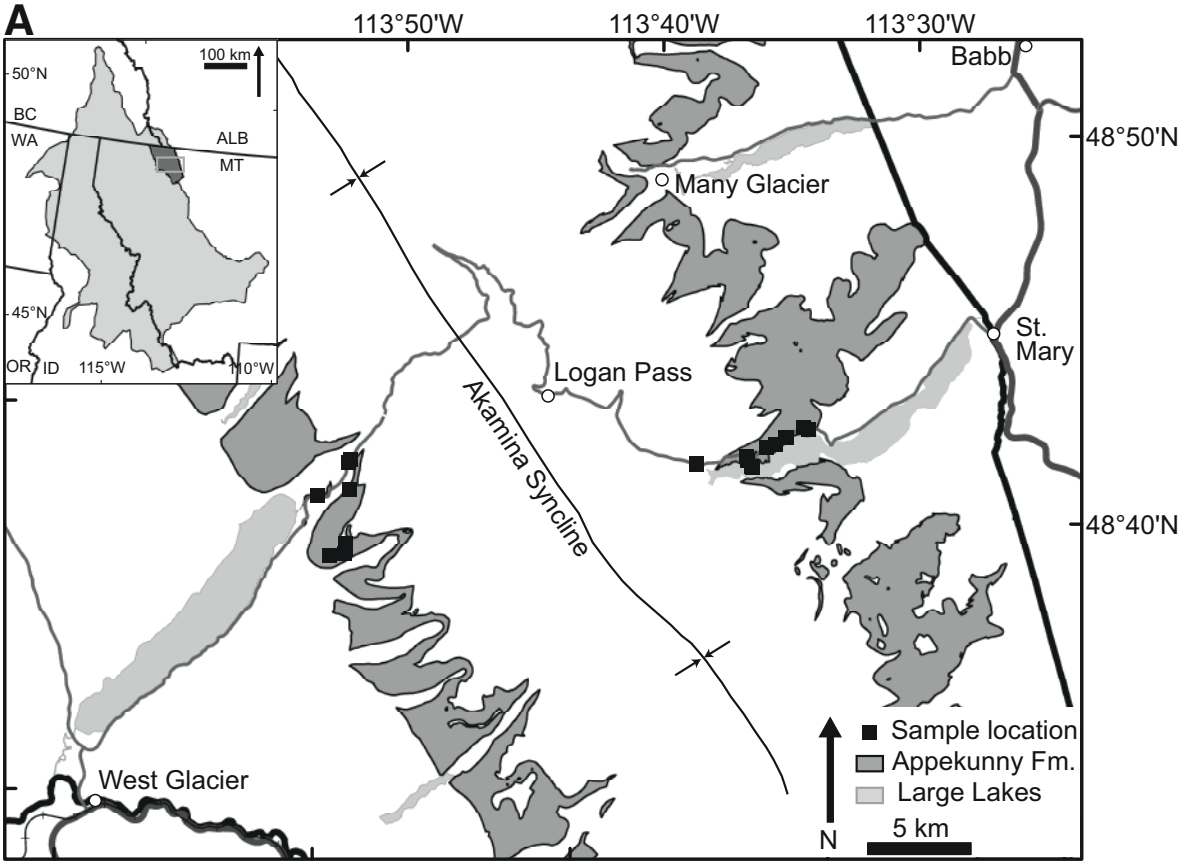

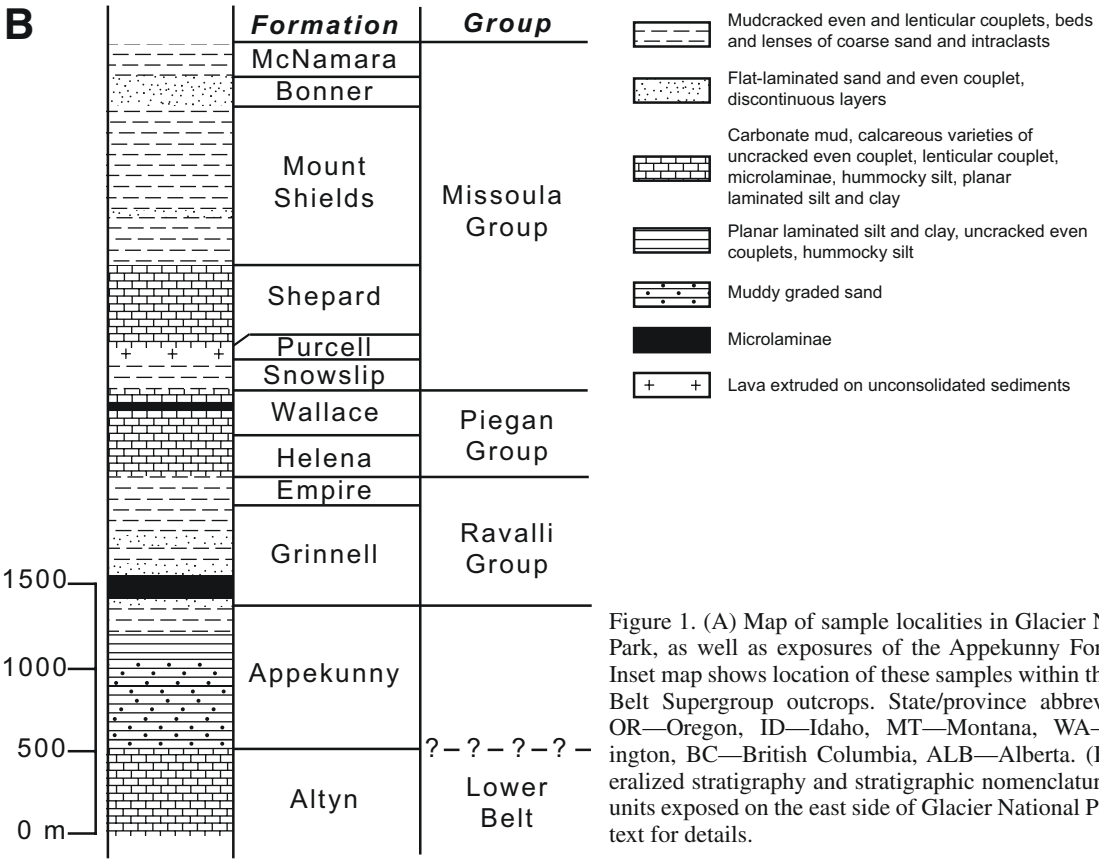

Figure 1. (A) Map of sample localities in Glacier National Park, as well as exposures of the Appekunny Formation. Inset map shows location of these samples within the larger Belt Supergroup outcrops. State/province abbreviations: OR—Oregon, ID—Idaho, MT—Montana, WA—Washington, BC—British Columbia, ALB—Alberta. (B) Generalized stratigraphy and stratigraphic nomenclature of the units exposed on the east side of Glacier National Park. See text for details.

The Belt Supergroup exposures in Glacier National Park provide a well-studied region of low metamorphic grade in which to investigate iron mineralogy, and they provide a different window into the redox status of the larger Belt Basin than previously studied samples from the Helena Embayment (Lyons et al., 2000; Planavsky et al., 2011; Stüeken, 2013). Based on sedimentological indicators, the strata in the park were predominantly deposited within storm wave base, even including intervals of subaerial exposure, from a much more proximal part of the basin (Winston and Link, 1993). For many of these shallower environments, the local water column should reflect a higher degree of influence by oxygen in the atmosphere, with the null expectation that local anoxic and/or H_2S-rich conditions would be tied to sedimentary pore fluids. However, the sedimentary units at Glacier National Park are well known for their brilliant green and red coloration, due to the variable and differential presence of reduced and oxidized iron-bearing minerals (Winston, 1986c). These differences have been hypothesized to reflect changing redox conditions even in these shallow waters (Stanley and Davies-Vollum, 2000), while others suggest they are diagenetic but broadly reflect syndepositional environments (Winston, 1986b, this volume). We focused our study of iron mineralogy, deposition, and preservation on the primarily green- and gray-colored Appekunny Formation, as well as the stratigraphic units above and below it, using a unique and powerful combination of techniques to assess iron mineralization including rock magnetics, light and electron microscopy, and synchrotron X-ray spectroscopy. Characterization of the iron mineralization of the Appekunny, Prichard, and Grinnell Formations provides support for new stratigraphic correlations of the Appekunny Formation across Glacier National Park and suggests that the shallow waters of the Belt Basin were similar to today with an oxic water column overlying suboxic to anoxic to H_2S-rich pore waters.

GEOLOGIC SETTING

The Belt Supergroup is composed of mixed siliciclastic and carbonate rocks in units that thicken from Glacier National Park to the west, reaching a maximum of 15–20 km (Winston and Link, 1993). Several tectonostratigraphic models for the origin and development of the Belt Basin have been proposed, including a large lake in an intercontinental rift (Winston, 1986b), a marine setting along the rifted margin of North America (Price, 1964), a lake or restricted marine setting from a remnant ocean basin (Hoffman, 1988), or a restricted marine/isolated lake setting due to supercontinental rifting (Luepke and Lyons, 2001; Lyons et al., 2000). Part of this debate is due to the preservation of shallow water and potentially fluvial sediments on the eastern edge of the basin, whereas a western margin was rifted away during the breakup of Rodinia (Stewart, 1972). Sediment provenance studies suggest a predominantly western source for the lower two thirds of Belt strata, with a predominately Laurentian source observed in Glacier National Park and the Helena Embayment (González-Álvarez et al., 2006; Ross and Villeneuve, 2003).

The Belt Supergroup has been divided into four main stratigraphic groups: the lower Belt, the Ravalli Group, the Piegan Group, and the Missoula Group (Whipple et al., 1984; Winston, 1986a, 2007; Fig. 1B). The lower Belt is primarily dark-colored mudstones and siltstones with iron sulfides, interpreted as deep basinal turbidites (Cressman, 1989). The Ravalli Group contains red and green mudstones and siltstones and light-colored sandstones deposited in shallower environments; some units and members display evidence of episodic subaerial exposure/playa environments (Winston, this volume; Winston and Link, 1993). The Piegan Group is composed of cyclic and/or graded dolomite, mudstone, and sandstone beds with common stromatolites, ooids, and molar tooth structures; it is interpreted to preserve the subtidal midshelf (Pratt, 2001) or underfilled lake deposits with less detrital input (Winston, 2007). The Missoula Group contains red to green mudstones, and pink quartz sandstones with thin intervals of carbonate and dark-gray mudstones interpreted to be alluvial, playa, and shallow subaqueous sequences (Winston and Link, 1993). Despite this well-recognized coarse stratigraphic architecture, more detailed stratigraphic correlations between different parts of the Belt Basin have been challenging, in part due to facies changes and local stratigraphic nomenclature. Notably, some have grouped the Appekunny Formation, composed of green and gray mudstones and siltstones, in the Ravalli Group with the overlying Grinnell Formation, composed of red and green mudstones and sandstones (e.g., Whipple et al., 1997, 1984; Fig. 1B). Others, due to its dramatic thinning and absence toward the west, have considered this unit to pass westward into the Prichard Formation, making it part of the lower Belt (Winston and Link, 1993), and/or it has been correlated with the Greyson Formation of the Helena Embayment (Harrison, 1972; Winston, 1986a), which is similarly nebulously assigned, sometimes with the lower Belt (Graham et al., 2012; Ross and Villeneuve, 2003; Winston and Link, 1993) and other times with the Ravalli Group (Harrison, 1972; Mudge et al., 1968). Observations of the stratigraphy, iron mineralogy, and geochemistry may help shed light onto these possible correlation schemes by providing additional data on the key transition from the east side of Glacier National Park to its western side.

The Belt Supergroup is variably well preserved across its present extent with known metamorphic gradients. In general, the degree of metamorphism increases to the west, with the best-preserved, lowest-temperature exposures in Glacier National Park and the Helena Embayment (Duke and Lewis, 2010). Within Glacier National Park, several studies have quantified the amount of metamorphism and postdepositional alteration of these rocks. Maxwell and Hower (1967) examined the structural changes of white mica (illite) from $1M_d$ or 1M polymorphs in low-grade samples to 2M polymorphs in more deeply buried samples, with the transition complete by the biotite isograd (Frey, 1987). Samples from the Appekunny Formation, Grinnell Formation, and Missoula Group in Glacier National Park were between 41% and 62% 2M polytype, suggesting sub-biotite-zone metamorphism. Eslinger and Savin

(1973) found a similar ranges from 21% to 61% 2M polytypes in samples from the Appekunny Formation, Grinnell Formation, and Helena Formation primarily from the east side of the park, which also increased with burial depth as interpreted from stratigraphic level. Oxygen isotope geothermometry of quartz and white micas indicated metamorphic temperatures between 225 °C and 310 °C, suggesting sub-biotite-zone to near-biotite zone (Eslinger and Savin, 1973). A new high-throughput technique using near-infrared spectroscopy to observe shifts in the Al-OH absorption band in white micas, which were correlated basinwide using other metamorphic studies (including those cited already), observed the Belt rocks of Glacier National Park to be some of the best preserved in the sub-biotite zone (Duke and Lewis, 2010).

Although the strata in Glacier National Park have not been as strongly heated and metamorphosed as those to the west in the Belt Basin, several observations of the mineralogy and petrography of the rocks within Glacier National Park have documented the effects of mineralization due to later diagenetic and/or metasomatic fluids. These observations include euhedral authigenic monazites in the Appekunny Formation and Grinnell Formation with dates ranging from 300 Ma to 1400 Ma, interpreted to reflect the protracted flow of basinal brines through these units (González-Álvarez et al., 2006). Peaks in age spectra at 1400 Ma, 1000–900 Ma, 600 Ma, and 300 Ma suggest an episodic nature to the metasomatism, which could be linked to continental-scale tectonic processes (González-Álvarez and Kerrich, 2010). Rare earth element abundances throughout the stratigraphic units in Glacier National Park highlight a mixture of near-primary compositions with two distinct alteration patterns that are more pronounced in sandstones, perhaps due to their greater permeability; the enrichment and depletion patterns suggest at least some of the alteration fluids were oxidizing and alkaline (González-Álvarez and Kerrich, 2010).

Previous studies have not directly examined the impact of these metasomatic fluids on the iron mineralogy in samples from Glacier National Park. However, some paleomagnetic measurements of the Grinnell Formation in Glacier National Park were noted to have overprints from phases of intermediate coercivity between 50 and 100 mT or Curie temperature between 210 °C and 610 °C, which were distinct from a component that demagnetized at over 665 °C (Vitorello and Van der Voo, 1977). The wide coercivity and temperature range given for the overprint component could be indicative of secondary hematite, maghemite, titanomagnetite, magnetite, pyrrhotite, or greigite, whereas the high-temperature component is uniquely hematite (Dunlop and Özdemir, 1997; Peters and Dekkers, 2003). The high-temperature component weakly passed a fold test, has a vector direction similar to other localities from the same time period, and thus was interpreted as primary (Vitorello and Van der Voo, 1977). Other samples of the Grinnell Formation in the northwestern portion of the park were not affected by these overprints and matched other samples across the Belt Basin, which also pass the field test for antiparallel reversals (Elston et al., 2002).

SAMPLE DESCRIPTIONS AND FIELD RELATIONSHIPS

Samples were collected in Glacier National Park, focusing on stratigraphic sections of the Appekunny Formation and extending into the overlying Grinnell Formation and the underlying Prichard Formation. To minimize effects on iron mineralogy possibly due to temporal and paleoenvironmental variation and/or heterogeneous distribution of altering fluid flow, samples were collected carefully from locations covering the entire Appekunny Formation on outcrops occurring on both the west and east limbs of the Akamina syncline, a broad SE-NW–trending structure running through Glacier National Park (Dahlstrom, 1970; Whipple et al., 1992; Fig. 1A).

The Appekunny Formation (Ross, 1959; Willis, 1902) has been divided into five informal members (Whipple et al., 1984) based on stratigraphic measurements on Apekuni Mountain in the Many Glacier region (Fig. 2B; Whipple et al., 1997). We revisited this type locality, and one of us (Slotznick) remeasured the stratigraphic section to describe these members in greater detail (Fig. 2A). Based on the Apekuni Mountain section, the descriptions of these members by J.W. Whipple, and previous field excursions by one of us (Winston) with J.W. Whipple, we identified and sampled outcrops of all five members on the east side of the park exposed along the Going-to-the-Sun Road. These sampled outcrops show very similar lithofacies and stratigraphy to the Many Glacier section, although we did not measure a detailed stratigraphic section along the Going-to-the-Sun Road. Observations and interpretations of sedimentary structures in these members vary slightly from previous authors and are described next for completeness.

Member 1 of the Appekunny Formation and the underlying Altyn Formation show a conformable gradational interbedded contact (over 10 m) of siltstone and argillite beds with carbonate layers. Based on Whipple et al. (1997), the base of member 1 was defined as a 1-m-thick greenish white quartz sandstone bed, above which sandstone continued to be interbedded with green siltstone and argillite for several meters. Member 1 consists of mostly planar, sometimes gently undulating laminated maroon siltstone with millimeter-thick laminae interstratified with equally thick layers of red claystone. Ripple cross-stratification is present at the millimeter to decimeter wavelength scale (Fig. 3A), with uncommon broad centimeter-tall hummocky cross-stratification. A thick quartz arenite sandstone bed in the middle of member 1 has been used as a key marker bed across the park (Whipple et al., 1984), and it is 24 m thick in the Apekuni Mountain section. Rare rip-up mud chips are found; overall, the member is interpreted as reflecting subaqueous sediment transport and deposition. Although mainly maroon to red in color, some grayish green intervals are observed; while sometimes discontinuous pinching out as lenses, others are distinct stratigraphic units that span large distances along strike. Samples of each colored lithotype were sampled and analyzed, with the maroon sample taken from lower in the succession than the green sample. Member 1 is 173 m thick

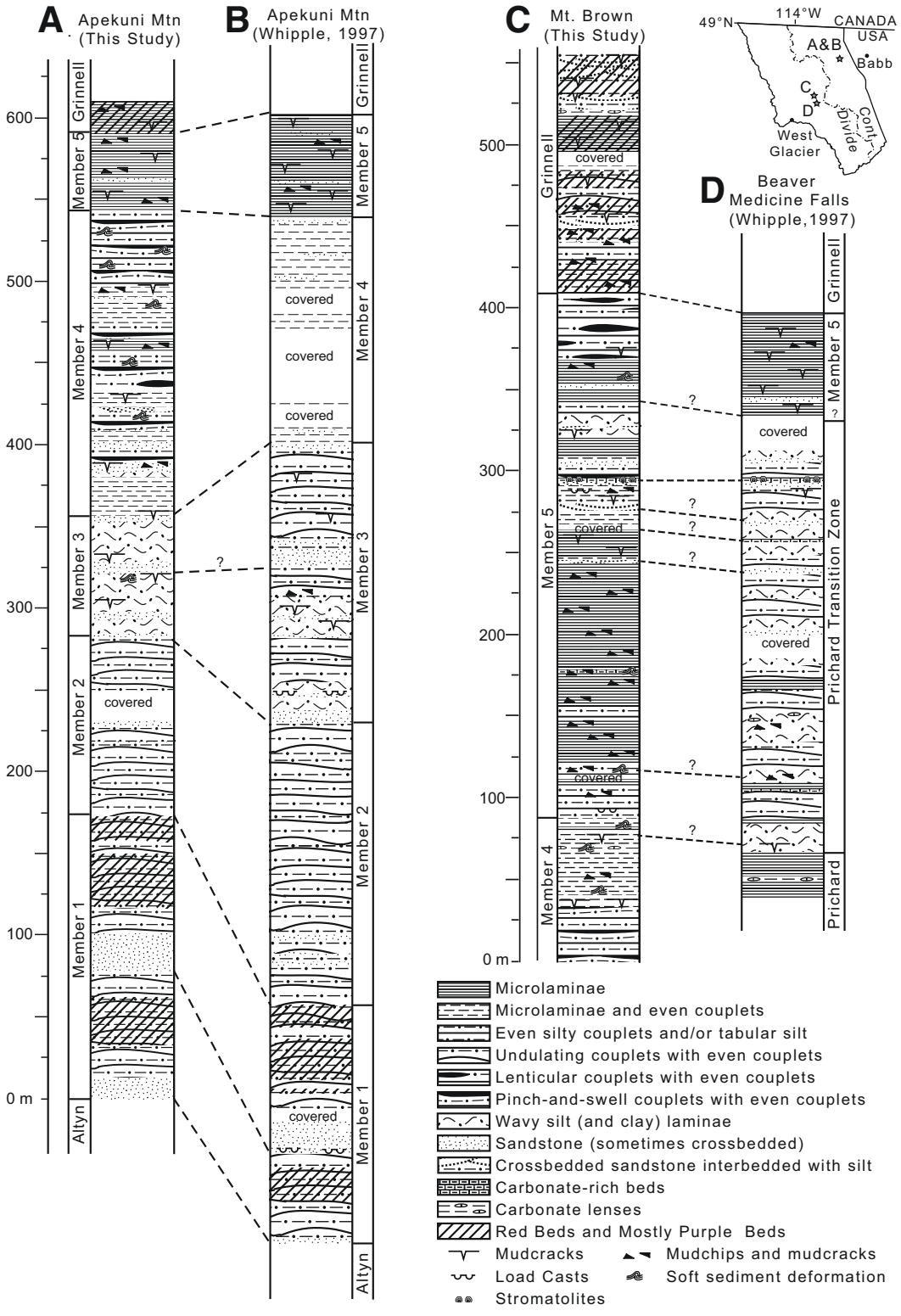

Figure 2. Stratigraphic columns of the Appekunny Formation. Scale is in meters and applies to all stratigraphic columns shown. Top-right inset: Map showing approximate locations of the stratigraphic columns in Glacier National Park; Cont. Divide—continental divide. (A) New stratigraphic section of the Appekunny Formation at the type section at Apekuni Mountain, Many Glacier. (B) Original stratigraphic section detailing the Appekunny Formation's five informal members at the type section of Apekuni Mountain, Many Glacier, from Whipple et al. (1997). (C) New stratigraphic section from the east face of Mount Brown, as well as new interpretation of the units present. Sedimentology is summarized in the text. (D) Stratigraphic section from Beaver Medicine Falls, Edwards Mountain, showing Prichard Formation and Prichard transition zone interpretations from Whipple et al. (1997).

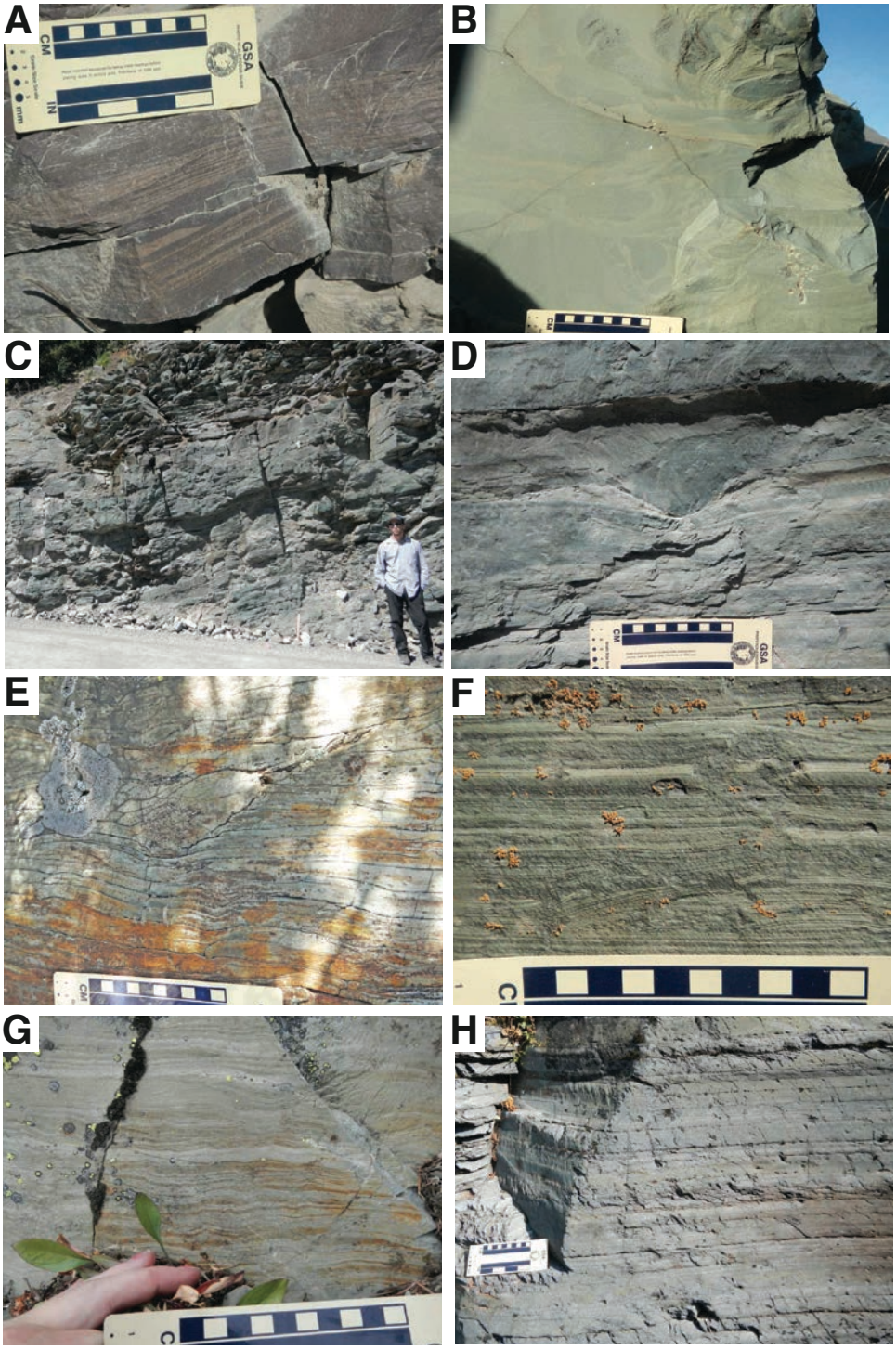

Figure 3. Photographs of Appekunny Formation member lithotypes and sedimentary structures along the Going-to-the-Sun Road. (A) Ripple cross-stratification in member 1. (B) Soft-sediment deformation load structures and plumose fracturing in member 2. (C) Large-scale hummocky cross-stratification in member 3. Person is 1.8 m for scale. (D) Centimeter-scale gutters in member 3. (E) Soft-sediment deformation and scour in lenticular beds of interbedded siltstone and claystone in member 4 on the east side. Note red iron oxides from weathering of iron sulfides. (F) Mud cracks and mud chips in flat even laminations of alternating siltstone and claystone in member 5 on the east side. (G) Lenticular siltstone and claystone couplets as well as soft-sediment deformation on east face of Mount Brown. (H) Gray siltstone and claystone even couplets with continuous beds rich in iron sulfides on west side of Mount Brown.

at Apekuni Mountain. *Horodyskia moniliformi*s was first found in the Appekunny Formation at Apekuni Mountain (Horodyski, 1982), and most fossils occur below the thick quartz sandstone marker bed in the middle of member 1 (Fedonkin and Yochelson, 2002; Retallack et al., 2013). Additional fossil examples have been collected in member 1 along the Going-to-the-Sun Road and at Rising Wolf Mountain in the Two Medicine region (Fedonkin and Yochelson, 2002; Retallack et al., 2013). One *Horodyskia* specimen was collected at Otokomi Mountain north of the Going-to-the-Sun Road, but no stratigraphic information is available for it (Horodyski, 1982).

Member 2 and member 1 have a gradational interbedded contact, with the top of member 1 set at the uppermost maroon beds (Whipple et al., 1992). Although very similar to member 1 in

lithology, member 2 notably has an increased proportion of green siltstone to mudstone, creating thicker beds up to a meter thick; these beds of well-sorted silt laminae often exhibit plumose fracturing. Planar to gently undulating to wavy lamination was observed on the centimeter to meter scale, with ripple cross-stratification and broad decimeter-scale hummock cross-stratification. Along the Going-to-the-Sun Road, multiple meter-thick beds display soft-sediment deformation structures, including loading and ball-and-pillow structures noted in the middle of member 2 (Fig. 3B). A few quartz sandstone beds are observed throughout the section, but they are thinner than those in member 1. Overall, member 2 is 145 m thick at Apekuni Mountain.

Member 3 contains several 2–5-m-thick pinkish brown quartz arenite sandstone beds and lenses/load structures; the lowest of these beds marks its base (Whipple et al., 1992). These arenite intervals contain common large millimeter-sized pyrite grains and goethite pseudomorphs after pyrite. Interbedded within the arenite sandstone and between these sandstone beds, there is grayish green siltstone with small amounts of claystone in thinly planar to wavy laminae. Most strikingly, this member contains common large hummocky cross-stratification up to a decimeter in height and up to meter scale in wavelength, and, in some locations, steep-walled decimeter-scale gutters cut into the underlying beds (Figs. 3C–3D). Additionally, member 3 differs from member 2 with increased claystone, the presence of common fining-upward cycles, and an orange-red weathering appearance of some intervals. Ripples and mud cracks are found throughout the member, the latter especially common near quartz arenite sandstone layers. No implied mechanism of formation is interpreted for the mud cracks; they could be either subaqueous or subaerial. Scattered rusty-weathering iron-oxide phases were observed in road-cut outcrop exposures, whereas fresh-cut samples revealed iron sulfides, suggesting the oxides are dominantly a recent near-surface weathering product. At Apekuni Mountain, member 3 is 72 m thick.

Member 4 is composed of green to dark greenish gray to dark- to medium-gray interbedded siltstone and claystone in millimeter- to centimeter-thick lenticular and pinch-and-swell layers. These are more silty than the microcouplets noted throughout the Prichard Formation (Winston and Link, 1993). Finely laminated, member 4 is fissile, weathering in thin plates, and it is poorly exposed. The base of the member is defined by the first occurrence of this thinly laminated siltstone (Whipple et al., 1992). Notable characteristics include the abundance of red iron oxides on parting surfaces, presumably from the exposure and surface weathering of iron sulfides. Scour pits and convolute bedding from soft-sediment deformation are also common and a defining characteristic (Fig. 3E). Hummocky cross-stratification is still present in this member, but it is less common and smaller in scale than member 3. Similarly, pinkish brown quartz arenite sandstone beds are still found in this unit. Mud cracks and mud chip breccias are also found throughout this member, often associated with quartz sandstone, but occasionally in green siltstone and claystone instead.

Member 5 is composed of fining-upward couplets (3 mm to 10 cm) and microlaminae (<3 mm) of planar laminated green siltstone and claystone. Abundant mud cracks and mud chip breccias (much more common than in member 4) highlight alternating subaerial desiccation and flooding of a shoreline muddy flat (Fig. 3F). The fine lamination of this unit results in weathering of the unit in thin plates, especially on Apekuni Mountain, where recent freeze-thaw cycles have made this unit be poorly exposed. Member 5 and member 4 have a complex gradational contact, with a few intervals of member 5–type beds found over a 75 m interval. The base of the contact is unclear from previous work, so it is defined here as transition from a majority of member 4–type intervals of pinch-and-swell, centimeter- to millimeter-thick laminations with scour pits, convolute bedding, and hummocky cross-stratification to even thinner beds with a predominance of microlaminae with mud cracks and mud chips characterizing member 5. This makes member 4 185 m thick at Apekuni Mountain, with a thin member 5 measuring 48 m in thickness.

Appekunny member 5 grades conformably up into the overlying Grinnell Formation. The base of the Grinnell Formation is defined by the lowest occurrence of red to purplish red mud-cracked claystone and siltstone beds (Whipple et al., 1984), although interbedded green and red beds continue for several tens of meters above this contact. Although the proportion varies, the Grinnell Formation contains more white quartz arenite sandstone lenticular beds throughout than the Appekunny Formation, and it preserves a wide range of shallow-water sedimentary structures from ripple marks and cross-stratification to mud cracks and mud chip/mud ball breccias.

Exposures of Appekunny member 5 continue on the west side of Glacier National Park (e.g., Fig. 2D). Here, it was interpreted to overlie the Prichard Formation with a thick transition zone containing wavy laminated and lenticular layers of calcareous claystone and siltstone as well as beds and lenses of quartz arenite and stromatolitic limestone (Whipple et al., 1997). Rare mud cracks were noted in a few intervals. The precise contact between the Appekunny Formation and Prichard Formation was not exposed within the park from previous stratigraphic descriptions, and it was postulated that Appekunny member 3 and 4 could even have extended to the west side of the park (Whipple et al., 1992, 1997). However, in the neighboring Whitefish and Flathead Range, the contact was suggested to be gradational, although there were questions about the identification of the Appekunny Formation in this locality (Harrison et al., 1998; Whipple et al., 1984).

A previously unpublished stratigraphic section was measured by coauthor Winston on the east side of Mount Brown, and it is shown here in Figure 2C. This locality is 3 km from a published section measured by J.W. Whipple at Beaver Medicine Falls, Edwards Mountain (Whipple et al., 1997; Fig. 2D), and it was measured in an effort to improve stratigraphic correlations within the park. Based on the new descriptions and definitions of the members of the Appekunny Formation from the type section and revisiting the east side of Mount Brown, we present here new stratigraphic interpretations for these units.

At the base of the section, there is an 89-m-thick package of medium-gray siltstone to dark-gray claystone microlaminae, subcentimeter-scale pinch-and-swell couplets, and even couplets (Fig. 3G). Soft-sediment deformation, including convolute bedding, is found throughout, sometimes producing clasts of the laminated mudstone. Mud cracks were observed near the top of this unit at 52 m and 76 m. Although entire laminae filled with abundant iron sulfides were not observed in the field, collected hand samples include very large (5 mm) iron-sulfide phases in various states of in situ oxidative weathering. We interpret this unit as member 4 due to its pinch-and-swell couplets, convolute bedding, and abundant iron oxides.

The transition to the next unit is gradational. The first 188 m of the unit are mainly composed of green, even microlaminae and microcouplets of siltstone to claystone, with common mud cracks and mud chip breccias. This unit's massive weathering is a striking feature, and it additionally contains several 10–60-cm-thick tabular siltstone beds. Several additional unique beds stand out from the siltstones and claystones in this unit. One calcareous bed weathers recessively and contains mud chips, mud cracks, and soft-sediment deformation features. In the upper portions, two 3-cm-thick medium-grained, well-rounded quartz sand beds with high-angle cross-bedding were observed.

A change in facies up section occurs, with 58 m of dark-gray interbedded siltstone and claystone and even pinch-and-swell couplets and microlaminae layers, as well as some hummocky cross-stratification in siltstones. Several 60-cm-thick, medium-grained sandstone beds with cross-stratification occur throughout the unit. This interval contains an increasing amount of carbonate, with several lenses of carbonate-rich mud chips and molar tooth hash. A 10-cm-thick stromatolitic limestone bed occurs at 295 m. Mud cracks with associated mud chips are rare, except in intervals near the sandstone beds. After the 58 m of wavy and pinch-and-swell layers, there is a return to green tabular siltstone beds, microlaminae, and lenticular to even siltstone to claystone couplets for another 75 m. Some intervals contain mud cracks and mud chips—textures that become more abundant near the top of the unit.

Here we interpret the entire 321 m as Appekunny member 5, with a small interval similar to Appekunny member 4 in this long complex transition. The upper portion of this has previously been identified as member 5 (Whipple et al., 1997), but due to the characteristics of the lower portion—with even couplets and microlaminae and abundant mud chip breccias—we think the lower portion should be grouped with member 5, even though it is below a small interbedded interval of pinch-and-swell beds. The new description of the type section at Apekuni Mountain highlights the complex long-gradational transition between these two members, so interbedded intervals of member 4–type facies within member 5 are not unexpected.

The top of this unit is marked by the first appearance of purple coloration in the even couplets of siltstone and claystone, with mud cracks and chips. This purple coloration appears interbedded with green-colored beds and lenses, as well as frequent thin quartz sand beds for at least 148 m. This is the contact of Appekunny Formation member 5 with the overlying Grinnell Formation.

The new Mount Brown stratigraphic column and facies detailed earlier highlight the abundance of mud cracks and mud chip breccias in the lower portion of the stratigraphy previously called the Prichard transition zone, as well as a lack of stratigraphically continuous laminae of abundant iron sulfides like those common in the Prichard Formation. Therefore, we argue that these strata do not represent classic Prichard Formation or Prichard transition zone, and we instead assign them to Appekunny members 4 and 5. While still in line with the interpretations by previous authors (Whipple et al., 1997) as a transitional facies, this interpretation extends Appekunny member 4 to the west side of the park and highlights a thickening of facies to the west consistent with the larger architecture of the Belt Basin. Although facies typical of the Prichard Formation—even couplets of gray siltstone and claystone with continuous layers of iron sulfides—were observed in outcrops on the west side of Mount Brown and along McDonald Creek, we found no clear evidence that these units are preserved on the east side of Mount Brown (Fig. 3H). Due to through-going structures and limited continuous exposure, it is difficult to determine the relative position of these samples within the stratigraphic columns to the east. The iron mineralogy and geochemistry of these units, however, may help to evaluate these possible correlations.

SAMPLING AND ANALYTICAL METHODS

Oriented block samples were collected by hiking off-trail from the Going-to-the-Sun Road, Glacier National Park in October 2012 and August 2014 (Fig. 1A). Metadata, including lithology, sedimentology, photographs, and global positioning system (GPS) locations, were also recorded for all samples. Samples covered all five members of the Appekunny Formation, the Grinnell Formation, and potentially the Prichard Formation (Table DR1[1]). Samples were cored using a nonmagnetic 25.4 mm diamond-edged drill bit, and sliced into 2–5-mm-thick specimen rounds using a saw with a nonmagnetic brass blade. Nondestructive rock magnetic experiments were performed on specimens using a 2G Enterprises SQuID magnetometer following the RAPID protocols, and these samples were analyzed using the RAPID Matlab (The Mathworks, Inc.) scripts (Kirschvink et al., 2008). Our protocol included measurements of alternating field (AF) demagnetization of the natural remanent magnetization (NRM), rotational remanent magnetization (RRM) acquisition and demagnetization, anhysteretic remanent magnetization (ARM) acquisition and demagnetization, isothermal remanent magnetization (IRM) acquisition and demagnetization, and backfield IRM acquisition. These analyses can be used to observe fundamental physical properties that can be used to distinguish different ferromagnetic

[1]GSA Data Repository Item 2016105, Table DR1: Detailed sample data for Glacier National Park samples, is available at www.geosociety.org/pubs/ft2016.htm, or on request from editing@geosociety.org or Documents Secretary, GSA, P.O. Box 9140, Boulder, CO 80301-9140, USA.

minerals (e.g., Peters and Dekkers, 2003). The destructive rock magnetic technique of Kappabridge thermal susceptibility was measured on neighboring specimens for a subset of the samples using an AGICO MFK1-FA Kappabridge, with the resulting data reduced using Cureval and Matlab scripts.

The same specimens that were run through nondestructive rock magnetic experiments were then made into polished thick or thin sections to provide a flat surface for optical, magnetic, and chemical imaging. Ultrahigh-resolution scanning SQuID microscopy (UHRSSM) was then performed on 11 of the sections with 100 μm pixels to locate ferromagnetic grains as regions for further analysis. Transmitted and reflected light microscopy was used to observe petrographic textures in all samples as well as identify additional target regions. Further petrographic observations were made using the Zeiss 1550VP field emission scanning electron microscope in the Caltech GPS Division Analytical Facility; this has a Robinson-type backscatter electron detector for imaging and a working distance of 8–9 mm. This instrument contains a paired Oxford X-Max SDD X-ray energy dispersive spectrometer (EDS) system used to determine X-ray spectra of elemental abundance at submicron-sized spots on 12 thin or thick specimens. This chemical information was important for confirming detections of chalcopyrite, galena, and sphalerite in addition to iron sulfides in many samples.

Synchrotron-based high-energy X-ray fluorescence (XRF) imaging was performed using beam line 10–2 at the Stanford Synchrotron Radiation Lightsource to characterize elemental abundances, including trace metals, in 21 thick or thin sections. Applied incident X-ray energies ranged from 20,200 eV to 10,000 eV, and standards for elements of interest were run at each beam time session with the same collection parameters. Synchrotron-based X-ray absorption near-edge spectroscopy (XANES/XAS) was paired with elemental imaging using beam line 14–3 and 2–3 at the Stanford Synchrotron Radiation Lightsource. X-ray absorbance spectroscopy (XAS) was performed in fluorescence mode at specific 2–4-μm-sized spots on 13 thin or thick sections to determine the chemical form of elements (oxidation state, orbital electronics, type and number of neighbors) while preserving textural information. Differences in the shape and K-edge of these absorption spectra allow us to easily distinguish between a wide range of Fe- and S- bearing minerals (Fleet, 2005; O'Day et al., 2004). Chalcopyrite and pyrrhotite have sufficiently similar S K-edge spectra that high-energy XRF, electron microscopy, and EDS were applied to confirm the presence of these minerals. The incident X-ray energy was set to energies around the sulfur absorption edge (2472 eV) and the iron absorption edge (7112 eV) using a Si (111) double crystal monochromator. At beam line 14–3, the monochromator energy was calibrated by setting the first thiol peak of a sodium thiosulfate powder to 2472.02 eV. At beam line 2–3, the monochromator energy was calibrated by setting the inflection point of a metallic Fe foil to 7112 eV. XRF elemental maps were processed using the MicroAnalysis Toolkit (Webb, 2011), and XAS data were processed using SIXPACK (Webb, 2005).

RESULTS

A wide array of iron-bearing minerals was observed in the samples collected from Glacier National Park, as summarized in Table 1. Importantly, bulk rock magnetic techniques provide a sensitive approach for finding and describing ferromagnetic minerals, but some of these techniques may not be diagnostic for a given phase. However, when coupled to petrography, phases can be confirmed, and, in certain cases, the mineralization sequence can be ordinated by crosscutting relationships or informed by grain shape. We discuss the results of these analyses first from the perspective of bulk techniques identifying iron minerals and then using petrographic (including chemical imaging) techniques.

The coercivity of remanence acquisition, determined using the derivative of the IRM, can be used to make ferromagnetic mineralogical determinations (Figs. 4A–4B; Heslop et al., 2002; Peters and Dekkers, 2003; Robertson and France, 1994). Notably, most of the samples share a similar mid-coercivity peak with a few additional different high-coercivity peaks present in some of the samples. Goethite is easily identified with coercivities over 1000 mT, and the range of 140–800 mT is generally indicative of hematite. However, the coercivity ranges for hematite, magnetite, titanomagnetite, greigite, and pyrrhotite overlap between 16 and 140 mT, though pyrrhotite, greigite, and hematite tend to have higher coercivities. Additionally, interpretations of coercivity data can be more difficult in natural samples where more than one ferromagnetic mineral is present. Thus, other techniques are valuable to provide confirmation and/or to separately identify these minerals.

The presence of RRM can be used to identify magnetic iron-sulfide phases like pyrrhotite, although the sensitivity limits are not well understood (Snowball, 1997; Thomson, 1990). Compared using B_{eff} (applied field × ratio of RRM to ARM), several samples in the west outcrops of member 4 indicated strong evidence for magnetic iron sulfides, $B_{eff} > \pm 20$ μT at 5 rps (revolutions per second) (Potter and Stephenson, 1986; Suzuki et al., 2006), while two samples of west side member 5 displayed weaker RRM signals, $B_{eff} > \pm 5$ μT at 5 rps (Fig. 4C). Notably, no samples on the east side showed any RRM, and thus they do not contain pyrrhotite. Additionally, all of the samples that had RRM displayed coercivity peaks greater than 100 mT, above the main middle-coercivity peak, suggesting that the lower common middle-coercivity mineral observed widely in Glacier National Park samples is magnetite.

In order to confirm the presence of magnetite and other iron-bearing minerals, Kappabridge thermosusceptibility experiments were used (Figs. 4E–4G). Magnetite was indicated by a drop in coercivity at 580 °C in all of the samples measured except one from west side outcrops of member 4. However, the Verwey transition at about –150 °C was not observed, suggesting either it was suppressed due to low abundance, with other phases dominating the signal, or that the magnetite contains a small weight percent titanium and could include titanomagnetite (Kozłowski et al., 1996; Moskowitz et al., 1998). Many of the samples showed the

TABLE 1. MINERAL IDENTIFICATIONS FROM SAMPLES OF THE APPEKUNNY, GRINNELL, AND PRICHARD FORMATIONS

	East side of Glacier National Park							West side of Glacier National Park		
	Member 1 (red)	Member 1 (green)	Member 2	Member 3	Member 4	Member 5	Grinnell	Prichard/ Member 4*	Member 4†	Member 5
Bulk techniques										
Magnetite		X	X	X	X	X		X	X	X
Hematite	X				X	X	X		X	X
Goethite	X	X	X	X			X		X	X
Pyrite			X		X			X		
Pyrrhotite								X	X	X
Textural techniques										
Goethite			X							
Iron oxide (generic)	X	X	X		X		X	X	X	X
Pyrite		X	X	X	X	X		X	X	X
Pyrrhotite								X	X	
Chalcopyrite		X				X		X	X	X
Galena						X			X	
Sphalerite		X			X	X		X	X	X
Nickel iron Monosulfide								X		
Cobalt arsenic sulfide									X	
Copper sulfide									X	
Ferric disulfide						X				
Chlorite	X	X	X	X	X	X		X	X	X
Barite	X	X	X	X	X				X	
Sulfate (generic)		X		X	X			X	X	

*Samples from the east face of Mount Brown and McDonald Creek.
†Samples from the west face of Mount Brown.

transformation of a nonmagnetic iron-bearing mineral into magnetite through a peak of increased susceptibility starting between 400 °C and 500 °C that dropped at 580 °C. This is interpreted as the decomposition of pyrite (Li and Zhang, 2005). Only one sample from the west side outcrop of member 4 displayed any sign of pyrrhotite's ferromagnetic to paramagnetic shift at its Curie temperature of 325 °C (Horng and Roberts, 2006; Minyuk et al., 2013). No low-temperature peaks hinted at the presence of goethite. Hematite is difficult to identify using Kappabridge thermal susceptibility due to its low susceptibility. The pure hematite Curie temperature transition is rarely seen in samples with other minerals like chlorite or elements like S or C, and the low-temperature Morin transition can be easily suppressed in submicron-size grains or with cation substitution (Bowles et al., 2010; Minyuk et al., 2011; Zhang et al., 2012). Indeed, Kappabridge experiments on samples containing hematite and carbon-, nitrogen-, or sulfur-bearing phases are hard to distinguish from those of pyrite decomposition, except that pyrrhotite sometimes forms during the cooling of pyrite, although cation substitutions can affect this process (Li and Zhang, 2005; Minyuk et al., 2011, 2013). Since no pyrrhotite was formed in our experiments, identification of pyrite using Kappabridge is only weak evidence for this mineral. The cooling curves are all much higher susceptibility than the initial heating curves in these thermosusceptibility experiments, often with a shifted peak toward lower temperatures of 200 °C to 550 °C. This suggests the decomposition of nonmagnetic minerals combining with other minerals to form titanomagnetite. This could be due to the reduction of paramagnetic hematite, the decomposition of ilmenite or other titanium-bearing minerals, and/or another less-well-understood process (Hrouda, 2003; Zhang et al., 2012).

Using an empirical rock magnetic procedure called the Fuller test, one can use the ratio of NRM:IRM to infer if the magnetization is detrital, chemical, or thermal in origin, especially when compared to the synthetic ARM:IRM relationships (Fuller et al., 1988, 2002). In sedimentary rocks deposited in approximately Earth-strength magnetic fields, NRM:IRM ratios of 1:1000 correspond to weak detrital magnetization, whereas ratios of 1:10 are typical of chemical remagnetization. This test was calibrated for magnetite and thus can only be applied to samples where the primary ferromagnetic mineral is magnetite. When applied to the samples from the Appekunny Formation that do not show RRM (no pyrrhotite) or large amounts of hematite, most of the samples show a NRM:IRM ratio of 1:1000, with a few slightly higher, but not near 1:10. These results suggest that the magnetite in these samples is detrital in origin. Results from the ARM modification of the Lowrie-Fuller test imply that this magnetite is single domain or pseudo–single domain, and is probably submicron (maximum less than 10 μm) in size (Johnson et al., 1975; Lowrie and Fuller, 1971; Xu and Dunlop, 1995).

To quantify the amount of magnetite in the samples, we used the saturation remanent magnetization measured using IRM

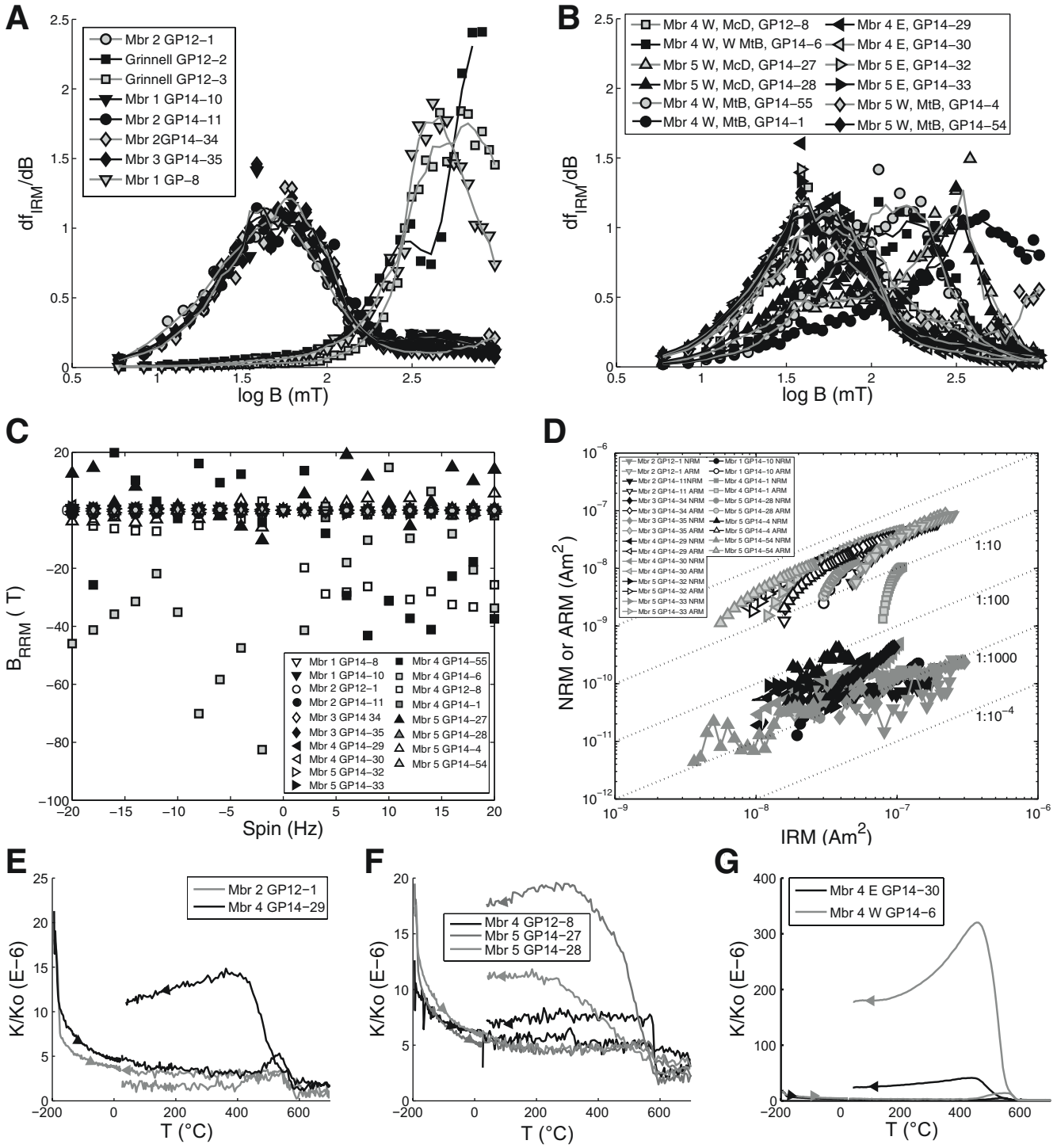

Figure 4. Bulk rock magnetic techniques. (A) Derivative of isothermal remanent magnetization (IRM) acquisition with respect to the applied field to determine coercivity of remanence acquisition for Grinnell Formation and Appekunny members 1–3. Abbreviations: f_{IRM}—normalized IRM; B—applied field. (B) Derivative of the IRM acquisition for members 4–5 separated by location in the park. Abbreviations: E—east side, W—west side, MtB—east face of Mount Brown, W MtB—west side of Mount Brown, McD—McDonald Creek. (C) Rotational remanent magnetization (RRM) of the Appekunny Formation samples to assess the presence or absence of magnetic iron-sulfide phases. (D) Fuller test to determine origin of magnetization in samples not showing RRM or dominant hematite. (E–G) KappaBridge thermal susceptibility (abbreviated as K) to determine mineralogy, with arrows showing direction of heating, including samples from the east side of the park (E), samples from the west side of the park (F), and some samples with strong signals (G). Sample stratigraphic member assignment is noted by number and by side of the park in part G. Data are normalized to an empty holder measurement (abbreviated as Ko).

acquisition. Magnetite has a saturation magnetization of 92 Am^2/kg (O'Reilly, 1984), and for magnetite, the ratio of the saturation remanence to the saturation magnetization has been calculated for a range of grain sizes in the famous Day plot (e.g., Day et al., 1977; Dunlop, 2002). Our samples are single domain or pseudo–single domain in size, so this ratio should be between 0.5 and 0.02. By mass-normalizing a measured saturation remanence, we can divide by the saturation magnetization of magnetite times a correction factor of the ratio of saturation remanence to saturation magnetization to get approximate percentages of magnetite in our samples (e.g., Klein et al., 2014). This calculation can only be done for samples where magnetite is the only or primary ferromagnetic mineral, and due to underlying assumptions, it is probably only accurate to an order of magnitude. Estimates range from tenths of a part per million (ppm) to tens of ppm of magnetite (depending on the ratio used), primarily for samples on the east side of the Glacier National Park, with one from the west side.

All mineralogical identifications using light and electron microscopy were confirmed chemically/structurally using synchrotron XAS and/or EDS spectra. All green or gray Appekunny Formation samples contained pyrite, but pyrrhotite was only observed in samples of member 4 (or Prichard Formation) on the west side of Glacier National Park (Fig. 5A). The presence of different sulfide phases with exotic trace-metal cations such as chalcopyrite, sphalerite, galena, nickel iron monosulfide, copper sulfide, and cobalt arsenic sulfide were also observed in many samples (Fig. 5C). Chalcopyrite and sphalerite occurred throughout the Appekunny Formation and on both sides of the park, while galena, nickel sulfides, and cobalt sulfides were only found in member 5 (east side) and member 4 (west side). Iron oxides were also identified in many of the samples throughout the Appekunny Formation and on both sides of the park, and they were primarily confirmed chemically using EDS. XAS at the Fe K-edge was used to identify the iron oxide as goethite in one sample from member 2 (Fig. 5B). Iron-bearing chlorite was also ubiquitous throughout the samples, identified by electron microscopy and EDS, as well as synchrotron XAS at the Fe K-edge (Fig. 5B). Sulfate phases were identified in many samples using S XAS (Fig. 5A), often with more than one sulfate salt present in a given sample. Electron microscopy and EDS characterized many of these sulfates as barite, but iron sulfates were also observed—these probably reflect the recent oxidative weathering of pyrite.

Using high-energy XRF maps, we were able to quantize the abundance of iron and trace metals for two of our samples (Table 2). XRF counts were correlated to mass based on standards measured during the same beam time session, then corrected for X-ray attenuation for each element and the rock matrix (assuming a homogeneous quartz lithology), then summed over a measured volume, and then divided by the sample density to find weight percent. This also implicitly assumes that a representative area was chosen for chemical imaging (Fig. 6). For all quantized elements, the values were remarkably similar across the park, often the same order of magnitude and similar to the second significant digit. However, comparison with previously measured bulk XRF and inductively coupled plasma–mass spectrometry (ICP-MS) elemental abundances of the Appekunny Formation (Table 2; González-Álvarez and Kerrich, 2010; González-Álvarez et al., 2006) suggests that while the textural XRF estimates for major elements (such as Fe) are within the expected range, the trace-element estimates are often 2–16 times more abundant than observed in bulk. This could be due to differential sample analysis, because given chemical imaging efforts were focused to a degree on reactive iron phases, and thus the abundance of trace metals contained within these texturally late iron-sulfide phases was overrepresented compared to background matrix.

Using these same XRF maps (Fig. 6), we estimated the volume percent of Fe-rich minerals such as iron sulfides and oxides. In this approach, the numbers of matrix pixels above a certain cutoff level of intensity of Fe signal were counted and divided by the total number of pixels in the XRF microprobe map to get a volume percent estimate (Table 2). This level was determined by cross-correlating the chemical maps with microscopy, XANES, and EDS to include all iron sulfides and oxides as identified in those regions but to exclude other minerals containing Fe such as chlorite. These calculations bear typical uncertainties associated with point-count estimates, but they avoid a certain degree of human error in phase identification (e.g., Johnson et al., 2014). Each pixel of the XRF maps represents the abundance over a volume of 10 µm by 10 µm by the thickness of samples, but they are actually 20 × 20 µm pixels based on the chosen measurement step size. In exporting these images from the MicroAnalysis Toolkit for point-counting processing, the pixels are redistributed at a finer scale across the map, which leads to some averaging between pixels. Therefore, to be counted in the volume estimation, the Fe-rich grains or aggregates must be sufficiently large in size, consisting of the majority of a 10 × 10 µm area (which has been further averaged in processing), and thus disseminate grains are not included in this estimate. In this manner, the presence of large aggregates of sulfide phases versus disseminated grains in the XRF mapped region will influence the volume percent estimation. Even with these caveats, similar volume percentages of Fe-rich minerals were attained for samples from both sides of the park, and these modal abundances were the same order of magnitude as modal abundances from point counting of other subbiotite-grade, organic-lean shales (e.g., Ferry, 1984, 2007).

From light and electron microscopy, many of the iron-bearing minerals show shapes or crosscutting textures that indicate their recrystallized and secondary nature. Much of the observed pyrite is euhedral, and it often is found in large nodular aggregations from samples throughout the park (e.g., Figs. 7B–7D). These nodules do not display evidence of differential compaction, unlike early nodules in the lower Belt's Newland Formation in the Helena Embayment (Schieber, 1989; Slotznick et al., 2015) and preserved macroscale soft-sediment deformation in the Appekunny Formation, implying a later diagenetic or metasomatic origin. Small aggregates of euhedral pyrite grains similar to pyrite framboids observed in modern anoxic and sulfidic sediments (Wilkin et al., 1996) were found in a few members on the

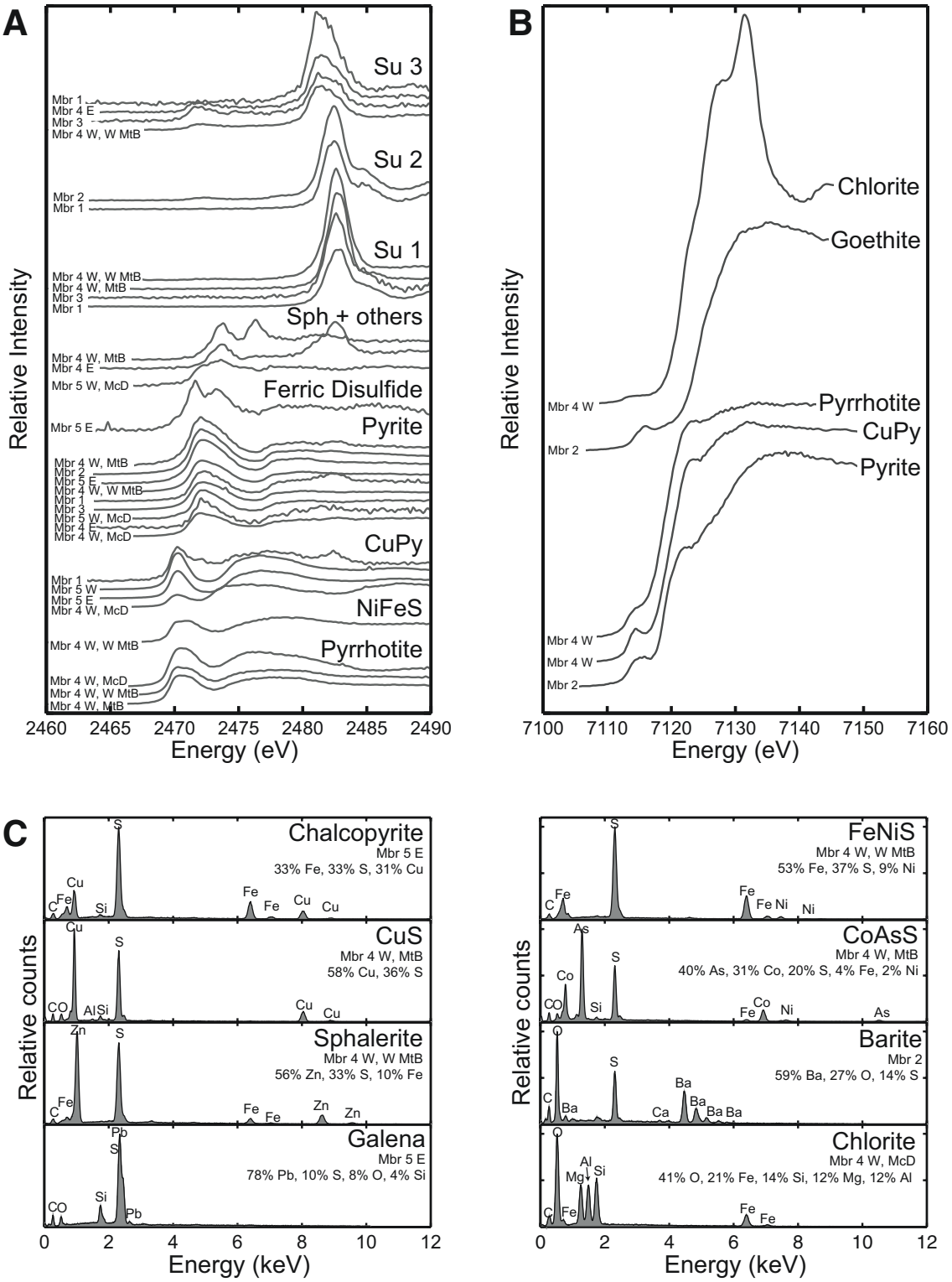

Figure 5. (A) End-member S X-ray absorption near-edge spectroscopy (XANES) spectra shown to exhibit mineralogical diversity found in each Appekunny member across different locations. Abbreviations for minerals: NiFeS—nickel iron monosulfide, CuPy—chalcopyrite, Sph—sphalerite, Su—sulfate. Abbreviations for location: E—east side, W—west side, MtB—east face of Mount Brown, W MtB—west side of Mount Brown, McD—McDonald Creek. Note that three different sulfate phases are indicated by small shifts in the K-edge position. (B) End-member Fe XANES spectra for two samples, one from member 2 and one from member 4 in McDonald Creek on the west side of Glacier National Park; CuPy—chalcopyrite. (C) X-ray energy dispersive spectrometer (EDS) spectra for examples of chalcopyrite, copper sulfide, sphalerite, galena, iron nickel sulfide, cobalt arsenic sulfide, barite, and chlorite. Same abbreviations as part A; chemical composition is included in wt% of chemical species. Samples were carbon coated for analysis, and carbon peaks result from this process.

TABLE 2. ELEMENTAL ABUNDANCES FROM X-RAY FLUORESCENCE MICROPROBE FOR SAMPLES OF THE APPEKUNNY FORMATION

Sample*	Member	Location*	Fe (wt%)	Ti (wt%)	Mn (wt%)	Cu (ppm)	As (ppm)	Zn (ppm)	Ni (ppm)	Fe-rich mineral (vol%)†
GP12-8, Reg1	Member 4	West, McD	2.01	0.232	0.042	21.3	42.7	106	131	0.2
GP12-1, Reg4	Member 2	East	3.54	0.213	0.000056	21.7	40.1	143	237	0.3
Average published Appekunny Formation data§			2.59 ± 0.55	0.294 ± 0.045	0.037 ± 0.024	12.4 ± 11.0	2.57 ± 1.41	58.3 ± 18.3	22.6 ± 8.33	

*Reg stands for region, East indicates east side of Glacier National Park, and West indicates west side of Glacier National Park; McD—McDonald Creek.

†Based on point counting X-ray fluorescence (XRF) map—this includes iron sulfides and oxides that represent most of a 6 or 13 µm square pixel.

§Data from silt and claystones of González-Álvarez et al. (2006) and González-Álvarez and Kerrich (2010), averaged with 1 population standard deviation, $n = 16$ for Fe, Ti, Mn, As, and Ni, and $n = 12$ for Cu and Zn.

east side of Glacier National Park (Fig. 7A), suggesting the much of the coarse euhedral pyrite could be simply recrystallized from an early diagenetic framboidal phase in these samples. These pyrite grains range in size from 1.5 to 10 µm average width/diameter, with a mean size of 4.3 µm (standard deviation = 1.7, n = 168), which is similar to other measured framboids and infilled framboids in modern sediments and in sediments throughout Earth history (Wilkin et al., 1996). In samples that contain multiple sulfide phases, various textural relationships were observed. In three samples, pyrite and pyrrhotite nodules contained small inclusions of chalcopyrite and sphalerite, often near veins or fractures within the crystal (Figs. 7B, 7C, and 7F); however, in other samples, sphalerite and chalcopyrite phases coexisted with pyrite as separate crystals. While pyrrhotite and pyrite were often found in the same samples, we did not observe clear crosscutting relationships between these phases. Sometimes, the pyrrhotite occurred in large aggregates with small grains of pyrite nearby, and sometimes pyrite was larger in grain size than the pyrrhotite (Fig. 7C). Surface weathering of iron oxides is present in many of the samples surrounding pyrite grains, and XAS showed at least one of these surrounding rims to be goethite (Fig. 7D). However, rims of chlorite and/or carbonate were also observed around iron sulfides on the west side of the park (Figs. 7E–7F). On the east side of the park, chlorite was present in the background fabric of the sample instead. Barite occurred in small isolated grains, sometimes with lath shapes, sometimes rounded (Fig. 7G), and sometimes as replacement/embayed domains with unclear origins (Figs. 7D and 7G). However, one sample contained barite intimately associated with the pyrite in space-filling patterns as well as small grains and rims (Fig. 7H).

DISCUSSION

Despite the well-preserved nature of the fine-grained siliciclastic Belt strata in Glacier National Park, secondary overprinting of the iron-bearing minerals in the Appekunny Formation was observed in all samples using a range of bulk and texture-specific techniques. Some of these alteration processes included recent (near) surface weathering, but many point to late diagenetic and/or metasomatic events. Nearly all pyrite has defined margins that crosscut fine-grained phases and reflect either recrystallization and coarsening of prior phases or mineralization from later fluids, although pyrite in exposures on the east side of the park appears generally better preserved, with several examples consistent with early diagenetic emplacement (Fig. 6A). Many samples contained sulfide phases enriched in As, Zn, Cu, Pb, Ni, and Co, which indicate the mobility of these metals as well as sulfur in postdepositional recrystallization events, possibly involving metasomatic fluids. Sulfide phases rich in these trace metals were observed throughout the Appekunny Formation on both sides of the park, suggesting any flow of altering fluids was not restricted to a particular stratigraphic member due to differential permeability, depth within the stratigraphy, and/or proximity to local structures. Samples with multiple sulfide phases in one nodule (found both in samples with and without pyrrhotite) emphasize the recrystallization of original iron minerals to incorporate trace metals. The impact of metasomatic fluids on the Appekunny Formation has been well noted by previous studies (González-Álvarez and Kerrich, 2010; González-Álvarez et al., 2006); however, less consideration has been given to how these processes have impacted the iron mineralogy, and the quality of interpretations of paleoenvironmental processes and chemistry of Belt Basin waters made from redox proxy data.

Pyrrhotite was found in several samples from the west side of Glacier National Park. Overall, the bulk magnetic technique of RRM appears to be a valuable indicator of the presence of magnetic iron sulfides, even in samples with multiple ferromagnetic components. Pyrrhotite was confirmed using XANES and EDS in all three samples that showed a strong RRM signal. Similarly, no pyrrhotite was found in samples that showed no RRM signal. Pyrrhotite was not found texturally in the two samples with moderate RRM signal ($\pm 20 > B_{eff} > \pm 5$ µT at 5 rps), but these grains could be very small with a weaker signal due to the overwhelming presence of other ferromagnetic minerals or another magnetic mineral could be capable of producing moderate RRM. The fact that pyrrhotite was only observed in samples from the west side of Glacier National Park, both in bulk and textural measurements, highlights local variations in metamorphic conditions in samples separated by only 26 km (though palinspastic reconstruction might restore a larger distance). Although modern examples of detrital pyrrhotite and early diagenetic pyrrhotite have been

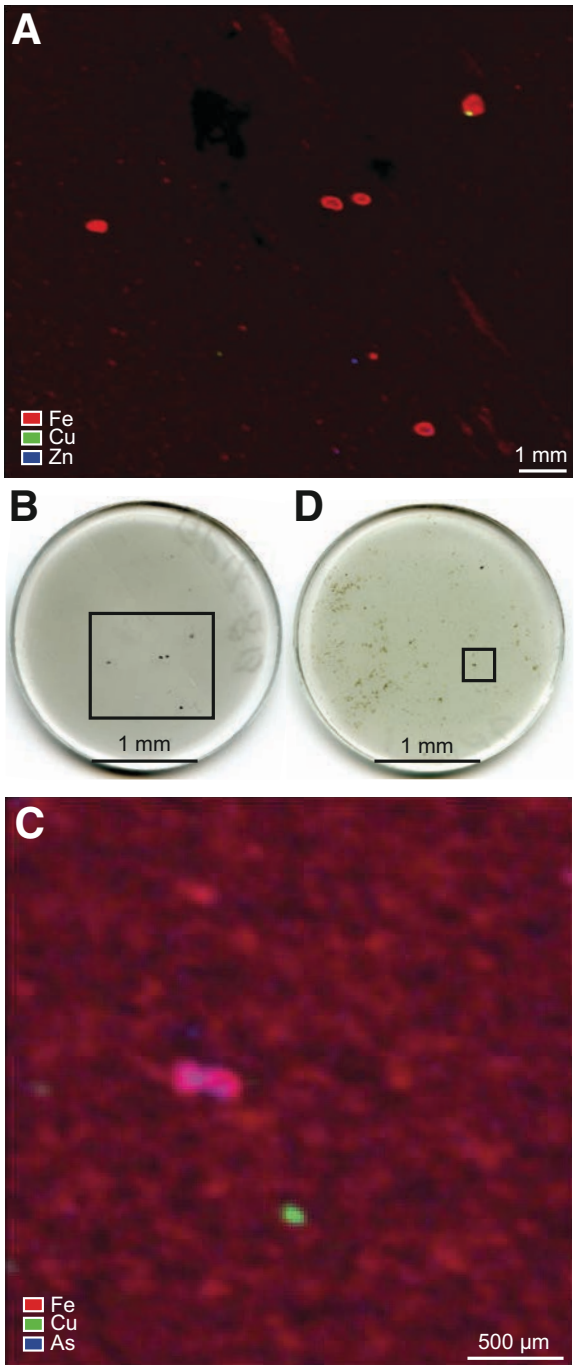

Figure 6. X-ray fluorescence (XRF) microprobe maps of elemental abundance used in quantification calculations as well as corresponding thin section scans. Each image has its own scale bar. (A) XRF for region 1 in GP12-8, member 4, west side on McDonald Creek. Color scales go from black at 0 to being brightly colored at maximum. Scale ranges are Fe = 0–4.69E–4 µg, Cu = 0–2.52E–5 µg, Zn = 0–9.20E–5 µg. (B) Scan of GP12-8 thin section showing region chosen for XRF map. (C) XRF for region 4 in GP12-1, member 2 east side. Color scales range from black at 0 to being brightly colored at maximum. Scale ranges are Fe = 0–4.38E–4 µg, Cu = 0–3.49E–6 µg, and As = 0–1.85E–6 µg. (D) Scan of GP12-1 thin section showing region chosen for XRF imaging.

found in unique environments (Horng and Roberts, 2006; Larrasoaña et al., 2007), much of the pyrrhotite in the rock record is interpreted to be due to the transformation of pyrite into pyrrhotite during metamorphism or precipitation from high-temperature fluids (e.g., Craig and Vokes, 1993; Hall, 1986; Weaver et al., 2002). In the presence of organic matter or a reducing environment, pyrite may transform to pyrrhotite beginning at 200 °C (Hall, 1986), with some experiments indicating that pyrrhotite can form at even lower temperatures depending on lithological constraints (Moreau et al., 2005; Raub et al., 2012). Although pyrrhotite formation is variable based on lithological constraints like organic matter (e.g., Carpenter, 1974), our new stratigraphic correlations suggest that the appearance of pyrrhotite is linked to different metamorphic conditions on the west side of the park and is not simply due to lithological differences between stratigraphic members. Although recent studies often screen for pyrrhotite (e.g., Asael et al., 2013; Planavsky et al., 2011), the presence of pyrrhotite makes interpreting iron speciation analyses tricky because it apportions iron to a highly reactive pool usually composed of oxides and carbonates; furthermore, it can be difficult to mass balance iron and sulfur, even when accounting for the iron in pyrrhotite, as the iron and sulfur budgets associated with pyrrhotization of pyrite in open systems remain unknown (Asael et al., 2013; Craig and Vokes, 1993; Piatak et al., 2007; Shannon and White, 1991; Zhou et al., 1995). Due to the lack of quantification for pyrrhotite, it is unclear the extent to which the pyrrhotite noted in these samples has impacted the bulk iron speciation data; however, the widespread observation of pyrrhotite on the west side of Glacier National Park shows that secondary processes have played a role in changing the iron geochemistry of these strata.

The presence of pyrrhotite only on the west side of the park is consistent with increasing burial metamorphism to the west, similar to the overall trend seen across the Belt Supergroup due to thickening of the section (Duke and Lewis, 2010; Winston and Link, 1993). Indeed, pyrrhotite has been widely observed in the Prichard Formation to the west of Glacier National Park, and linked via geochemistry to the metamorphic transformation of pyrite (Luepke, 1999; Luepke and Lyons, 2001). Within Glacier National Park, the appearance of pyrrhotite could be linked to transformations at deeper burial depths in a reducing environment, probably an open system, but distinct fluids could also have delivered and/or removed dissolved iron and sulfide to precipitate pyrrhotite (e.g., Hall, 1986). Supporting this suggestion is the observation that cobalt arsenic base metal sulfides from the west side of the park are closely texturally associated with the pyrrhotite. Notably, the chlorite rims surrounding the pyrrhotite and pyrite aggregates on the west side of the park suggest an even later transformation (and redox change) of iron from sulfides into a mixed-valence silicate phase. This highlights the increased mobility of iron between different minerals on the west side of the park, explainable by either of the mechanisms detailed above, but in a second alteration event after pyrrhotite had already formed.

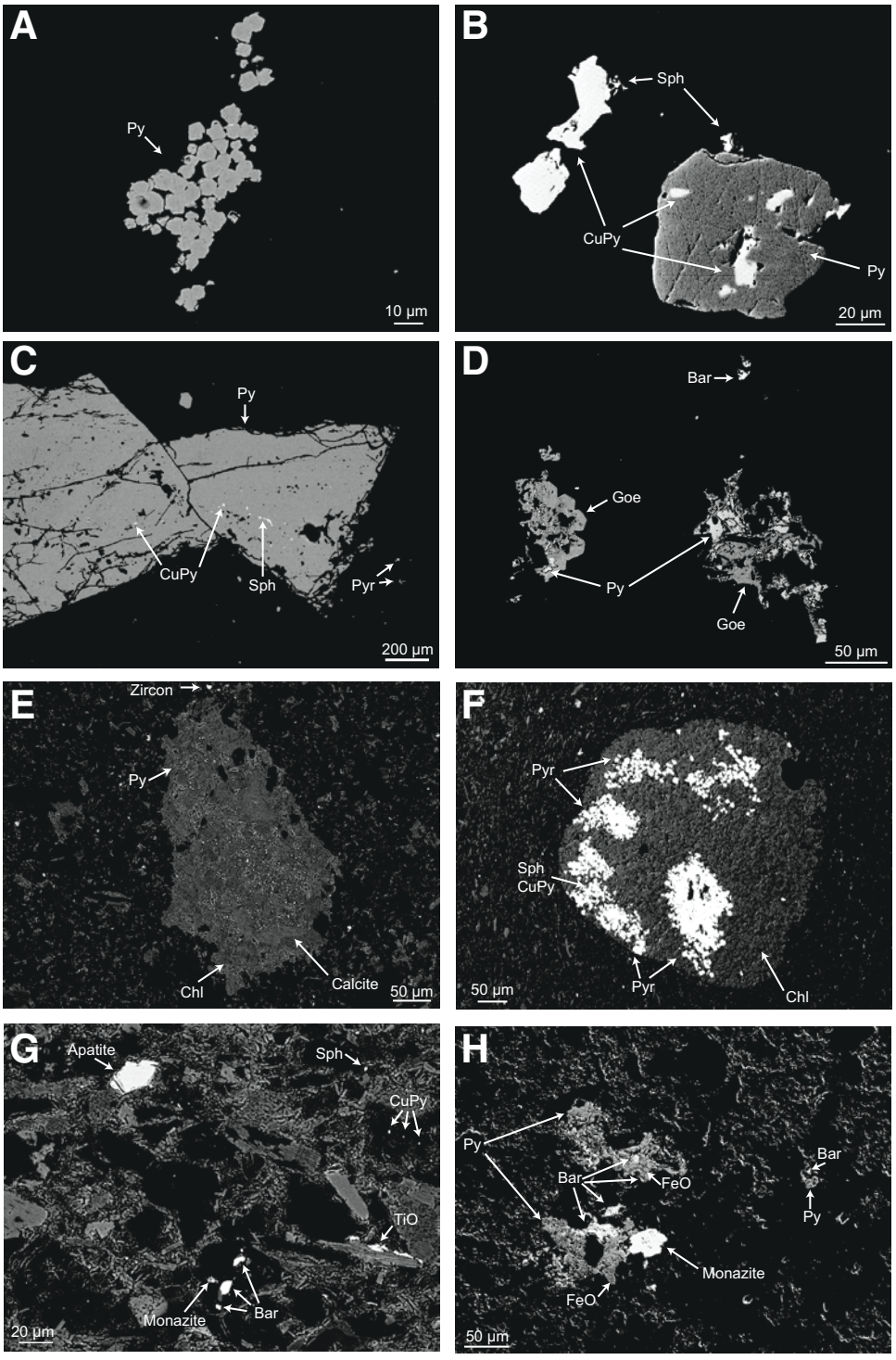

Figure 7. Backscatter electron and scanning electron images, each with own scale bar. Abbreviations for labeled minerals: Py—pyrite, CuPy—chalcopyrite, Sph—sphalerite, Pyr—pyrrhotite, Goe—goethite, Bar—barite, Chl—chlorite, TiO—titanium oxide, FeO—iron oxide (generic). (A) Small framboidal pyrite grains in Appekunny member 3 (GP14-35). (B) Pyrite grain with inclusions of chalcopyrite and sphalerite as well as neighboring chalcopyrite grain in Appekunny member 5, east side outcropping (GP14-32). (C) Large nodular pyrite grain with small neighboring pyrrhotite grains in member 4/Prichard, west side of park (GP14-6). (D) Goethite surrounding pyrite grains interpreted as replacement of euhedral recrystallized nodules in member 2 (GP12-1). (E) Small pyrite grains within carbonate nodule, rimmed by chlorite in member 5, west side of park (GP14-27). (F) Chlorite rim replacing pyrrhotite nodule in member 4/Prichard, west side of park (GP12-8). (G) Individual barite grains far from sulfides or other sulfates in member 1 (GP14-10). (H) Barite rimming pyrite and iron oxides filling spaces as well as replacing grains in member 2 (GP14-11).

One of the most interesting iron mineralogical findings in this study was the discovery of nearly ubiquitous submicron-size magnetite across all of the Appekunny Formation in all members. Results from the rock magnetic Fuller test suggest that this magnetite is detrital due to its low ratio of NRM:IRM, whereas chemical precipitation would be expected to have a much stronger magnetization than was observed. The evidence for detrital magnetite is important because it represents a significant delivery process of iron into the system that is not directly linked to the redox chemistry of the depositional waters. In bulk geochemical iron speciation measurements, abundant preserved detrital magnetite would skew results toward an interpretation of ferruginous

waters; however, the amounts of magnetite present in our samples are too low to dramatically impact the results of bulk geochemical extraction techniques. The observations of detrital iron fluxes provide an important view of the iron systematics in the basin by documenting an important supply of highly reactive iron to the basin (e.g., Canfield and Berner, 1987). Furthermore, the preservation of at least some of this magnetite suggests that a large anoxic H_2S-rich zone (either in the water column or as sedimentary pore fluids), if present during deposition of the strata in Glacier National Park, was not sufficient to scavenge all this highly reactive iron to form pyrite (Canfield and Berner, 1987; Lyons and Severmann, 2006). Additionally, neither the water column nor pore fluids were sufficiently rich in ferrous iron to recrystallize detrital magnetite and generate a chemical remanent magnetization (e.g., Skomurski et al., 2010).

The presence of shallow-water hematite-bearing red units in member 1 of the Appekunny Formation, as well as in the overlying Grinnell Formation, highlights the presence of oxygen in the atmosphere and shallow waters. All of the units in the Appekunny Formation of Glacier National Park represent relatively shallow-water environments of the Belt Basin, and based on sedimentary structures from orbital water motion, long-lived stratification of the water column seems unlikely. However, the framboidal pyrite in samples from the east side of Glacier National Park (and perhaps even much of the recrystallized pyrite seen elsewhere) suggests the precipitation of early diagenetic pyrite during organic diagenesis. Thus, pyrite is reasonably interpreted as an indicator of primary anoxic and sulfidic sedimentary environments in the Belt Basin, but, based on the constraints noted earlier herein suggesting oxic, nonstratified conditions in shallow waters, it seems likely that these conditions were effectively limited to sediment pore waters. Detrital iron oxides likely provided an important source of highly reactive iron for pyrite formation during organic diagenesis (Canfield and Berner, 1987; Raiswell and Canfield, 1998). Based on our observations, the shallow waters and sediments of the Belt Basin preserved in Glacier National Park do not show any signs of being anoxic and sulfur-poor (i.e., ferruginous conditions) as was hypothesized for older, more distal sediments further south in the basin (Planavsky et al., 2011). The barite closely associated with pyrite in space-filling patterns (Fig. 7H) suggests at least some of the barite precipitated from diagenetic and/or metasomatic reactions with deep fluids and may not be representative of sulfate in the depositional waters (Griffith and Paytan, 2012; Hanor, 2000). The presence of authigenic replacement barite not associated with iron sulfides found in many of the samples (Figs. 7D and 7G) could in principle record postdepositional oxidizing fluids, although these micron-scale grains may instead reflect precipitation during early organic diagenesis, associated with vacillating redox fronts of sulfate reduction with pore-fluid sulfate sourced from bottom waters (Griffith and Paytan, 2012; Koski and Hein, 2004). Water column or detrital barite could be a component of our samples, but no lath-shaped euhedral barite was identified, and while rounded grains were observed (Fig. 7G), they often occurred near barite displaying replacement or embayed textures. This suggests much of either the water column or detrital barite was recrystallized after deposition.

Ultimately, the iron mineralogy and geochemistry of the Appekunny Formation and surrounding formations suggest a redox structure of (relatively) shallow mid-Proterozoic sedimentary basins that was similar to today, with detrital iron fluxes carried through oxygenated waters, wherein sedimentary environments with sufficient organic carbon loads exhausted their supply of O_2 and underwent anaerobic respiratory metabolisms that promoted sulfidic pore fluids and the production of diagenetic pyrite. Additionally, from the data generated in this study, we can link evidence for oxygenated waters directly to outcrops known to contain the early macroscale fossil *Horodyskia moniliformis*, a putative (aerobic) eukaryote. Understanding the depths in the Belt Basin to which water was oxygenated and whether anoxic and sulfidic conditions emerged from the sediments into the water column in more distal sedimentary settings (Gellatly and Lyons, 2005; Luepke and Lyons, 2001; Slotznick et al., 2015), or whether the water column instead became anoxic and ferruginous (Planavsky et al., 2011), remains a priority for future work.

Although our iron mineralogy analyses shed light onto questions about redox and geochemistry of the Belt Basin, they are not straightforward in aiding stratigraphic correlations across Glacier National Park. Sulfides rich in Zn, Cu, and Pb were found on both sides of the park, and they do not appear to be restricted to any single stratigraphic member. Similarly, pyrrhotite appears to be a characteristic of the west side of Glacier National Park and is not restricted to a single member. It is noteworthy that the abundance of pyrrhotite (as well as pyrite) in samples on the west side of Glacier National Park was distinct between different units. Appekunny member 4/Prichard-like lithologies from the west face of Mount Brown and McDonald Creek contained abundant pyrrhotite, as did samples in proposed member 4 on the east face of Mount Brown. Samples from member 5 in McDonald Creek and from proposed member 5 on the east face of Mount Brown contained smaller proportions or no pyrrhotite. This suggests a stratigraphic link between samples on the west side Mount Brown and the better-studied McDonald Creek region and supports the hypothesis that the strata on the east face of Mount Brown are metamorphosed equivalents of member 4, maybe even the same member as the more Prichard-like samples on the west face and in McDonald Creek. Additionally, member 4 siltstones and claystones on the east side of the park contained abundant pyrite, which could reflect the mineralogical progenitor of the abundant pyrrhotite seen on the west side of the park in these ambiguously correlated units.

CONCLUSION

The Appekunny Formation of Glacier National Park is an excellently preserved shallow-water unit that, while complicated by postdepositional processes, still contains records of primary redox chemistry of the Belt Basin during mid-Proterozoic time

when macroscopic life was emerging. From our iron mineralogy and chemical observations, we propose that the shallow waters in the Belt Basin were oxygenated, but with underlying suboxic H_2S-rich pore waters that promoted precipitation of pyrite. This water chemistry and these redox processes are similar to those of shallow sedimentary basins today, and they may help to explain why these rocks are notably fossiliferous (e.g., Horodyski et al., 1989), as many of the preserved biota are interpreted as (different) aerobic organisms. In the sedimentary rocks of Glacier National Park, most of the strata capture paleoenvironments that would have been habitable to diverse sets of aerobic organisms. Our interpretations of the paleoenvironment in Glacier National Park provide a geochemical constraint on paleoredox conditions that help support the hypotheses from many paleontologists that some of the macroscale and microscale fossils found in Glacier National Park and in the rest of the Belt Basin were early eukaryotes (e.g., Adam et al., 2014; Fedonkin and Yochelson, 2002; Horodyski, 1993; Retallack et al., 2013; Walter et al., 1976, 1990). It is possible that portions of the Belt Basin could have been anoxic or euxinic (e.g., Slotznick et al., 2015) in either a stratified or locally heterogeneous manner, but these paleoredox constraints are distinct in time and record deeper-water environmental settings than the fossiliferous units focused on in this work. Iron mineralogy preserved in Precambrian rocks is rich and complex, with the possibility of many different redox and phase transformations. By combining textural and bulk techniques, it is possible to untangle the iron phases to get a picture of key redox processes operating in the environment and the postdepositional processes that have served to complicate our interpretation of that history.

ACKNOWLEDGMENTS

We thank Rob Thomas, Tim Lyons, Austin Chadwick, and Steven Skinner for assistance with stratigraphic measurements and sample collections under National Park Service (NPS) collection permits GLAC-2012-SCI-0195 and GLAC-2014-SCI-0008. Thanks also go to Jim Sears, Johnny MacLean, Erik Sperling, and an anonymous reviewer for helpful comments that greatly improved the manuscript. Support for this work was provided by the Agouron Institute, a Tobacco Root Geological Society scholarship, a Belt Association student research grant, a Geological Society of America student research grant, the National Aeronautics and Space Administration (NASA) Exobiology program (Fischer), the David and Lucile Packard Foundation (Fischer), the National Science Foundation Graduate Research Fellowship program (Slotznick), a NASA Earth and Space Science fellowship (Slotznick), and a Philanthropic Educational Organization (PEO) Scholar Award (Slotznick). Portions of this research were carried out at the Stanford Synchrotron Radiation Lightsource, a directorate of the SLAC National Accelerator Laboratory and an Office of Science User Facility operated for the U.S. Department of Energy Office of Science by Stanford University.

REFERENCES CITED

Adam, Z., Mogk, D., Skidmore, M., and Butterfield, N., 2014, Microfossils from the Greyson Formation, Lower Belt Supergroup: Support for early Mesoproterozoic biozonation: Geological Society of America Abstracts with Programs, v. 46, no. 5, p. 71.

Anderson, H.E., and Davis, D.W., 1995, U-Pb geochronology of the Moyie sills, Purcell Supergroup, southeastern British Columbia: Implications for the Mesoproterozoic geological history of the Purcell (Belt) Basin: Canadian Journal of Earth Sciences, v. 32, no. 8, p. 1180–1193, doi:10.1139/e95-097.

Asael, D., Tissot, F.L., Reinhard, C.T., Rouxel, O., Dauphas, N., Lyons, T.W., Ponzevera, E., Liorzou, C., and Chéron, S., 2013, Coupled molybdenum, iron and uranium stable isotopes as oceanic paleoredox proxies during the Paleoproterozoic Shunga event: Chemical Geology, v. 362, p. 193–210, doi:10.1016/j.chemgeo.2013.08.003.

Bowles, J., Jackson, M., and Banerjee, S., 2010, Interpretation of low-temperature data: Part II. The hematite Morin transition: IRM Quarterly, v. 20, p. 1–10.

Canfield, D., 1998, A new model for Proterozoic ocean chemistry: Nature, v. 396, no. 6710, p. 450–453.

Canfield, D.E., and Berner, R.A., 1987, Dissolution and pyritization of magnetite in anoxic marine sediments: Geochimica et Cosmochimica Acta, v. 51, no. 3, p. 645–659, doi:10.1016/0016-7037(87)90076-7.

Carpenter, R.H., 1974, Pyrrhotite isograd in southeastern Tennessee and southwestern North Carolina: Geological Society of America Bulletin, v. 85, no. 3, p. 451–456, doi:10.1130/0016-7606(1974)85<451:PIISTA>2.0.CO;2.

Cloud, P.E., 1968, Atmospheric and hydrospheric evolution on the primitive Earth: Science, v. 160, no. 3829, p. 729–736, doi:10.1126/science.160.3829.729.

Craig, J.R., and Vokes, F.M., 1993, The metamorphism of pyrite and pyritic ores: An overview: Mineralogical Magazine, v. 57, p. 3–18, doi:10.1180/minmag.1993.057.386.02.

Cressman, E.R., 1989, Reconnaissance Stratigraphy of the Prichard Formation (Middle Proterozoic) and the Early Development of the Belt Basin, Washington, Idaho, and Montana: U.S. Geological Survey Professional Paper 1490, 80 p., 4 plates.

Dahlstrom, C.D., 1970, Structural geology in the eastern margin of the Canadian Rocky Mountains: Bulletin of Canadian Petroleum Geology, v. 18, no. 3, p. 332–406.

Day, R., Fuller, M., and Schmidt, V., 1977, Hysteresis properties of titanomagnetites: Grain-size and compositional dependence: Physics of the Earth and Planetary Interiors, v. 13, no. 4, p. 260–267, doi:10.1016/0031-9201(77)90108-X.

Dong, L., Xiao, S., Shen, B., and Zhou, C., 2008, Silicified *Horodyskia* and *Palaeopascichnus* from Upper Ediacaran cherts in South China: Tentative phylogenetic interpretation and implications for evolutionary stasis: Journal of the Geological Society, London, v. 165, no. 1, p. 367–378, doi:10.1144/0016-76492007-074.

Duke, E.F., and Lewis, R.S., 2010, Near infrared spectra of white mica in the Belt Supergroup and implications for metamorphism: The American Mineralogist, v. 95, no. 7, p. 908–920, doi:10.2138/am.2010.3281.

Dunlop, D.J., 2002, Theory and application of the Day plot (Mrs/Ms versus Hcr/Hc): 1. Theoretical curves and tests using titanomagnetite data: Journal of Geophysical Research–Solid Earth (1978–2012), v. 107, no. B3, p. EPM 4-1–EPM 4-22.

Dunlop, D.J., and Özdemir, Ö., 1997, Rock Magnetism: Fundamentals and Frontiers: Cambridge, UK, Cambridge University Press, 596 p., doi:10.1017/CBO9780511612794.

Elston, D., Enkin, R., Baker, J., and Kisilevsky, D., 2002, Tightening the Belt: Paleomagnetic-stratigraphic constraints on deposition, correlation, and deformation of the Middle Proterozoic (ca. 1.4 Ga) Belt-Purcell Supergroup, United States and Canada: Geological Society of America Bulletin, v. 114, no. 5, p. 619–638, doi:10.1130/0016-7606(2002)114<0619:TTBPSC>2.0.CO;2.

Eslinger, E.V., and Savin, S.M., 1973, Oxygen isotope geothermometry of the burial metamorphic rocks of the Precambrian Belt Supergroup, Glacier National Park, Montana: Geological Society of America Bulletin, v. 84, no. 8, p. 2549–2560, doi:10.1130/0016-7606(1973)84<2549:OIGOTB>2.0.CO;2.

Evans, K.V., Aleinikoff, J.N., Obradovich, J.D., and Fanning, C.M., 2000, SHRIMP U-Pb geochronology of volcanic rocks, Belt Supergroup, western Montana: Evidence for rapid deposition of sedimentary strata: Canadian Journal of Earth Sciences, v. 37, no. 9, p. 1287–1300, doi:10.1139/e00-036.

Fedonkin, M.A., and Yochelson, E.L., 2002, Middle Proterozoic (1.5 Ga) *Horodyskia moniliformis* Yochelson and Fedonkin, the oldest known tissue-grade colonial eukaryote: Smithsonian Contributions to Paleobiology 94, 29 p.

Ferry, J.M., 1984, A biotite isograd in south-central Maine, USA: Mineral reactions, fluid transfer, and heat transfer: Journal of Petrology, v. 25, no. 4, p. 871–893, doi:10.1093/petrology/25.4.871.

Ferry, J.M., 2007, The role of volatile transport by diffusion and dispersion in driving biotite-forming reactions during regional metamorphism of the Gile Mountain Formation, Vermont: The American Mineralogist, v. 92, no. 8–9, p. 1288–1302, doi:10.2138/am.2007.2429.

Fleet, M.E., 2005, XANES spectroscopy of sulfur in earth materials: Canadian Mineralogist, v. 43, no. 6, p. 1811–1838, doi:10.2113/gscanmin.43.6.1811.

Frey, M., 1987, Low Temperature Metamorphism: Glasgow, Blackie, 351 p.

Fuller, M., Cisowski, S., Hart, M., Haston, R., Schmidtke, E., and Jarrard, R., 1988, NRM-IRM(s) demagnetization plots—An aid to the interpretation of natural remanent magnetization: Geophysical Research Letters, v. 15, no. 5, p. 518–521, doi:10.1029/GL015i005p00518.

Fuller, M., Kidane, T., and Ali, J., 2002, AF demagnetization characteristics of NRM, compared with anhysteretic and saturation isothermal remanence: An aid in the interpretation of NRM: Physics and Chemistry of the Earth, v. 27, no. 25–31, p. 1169–1177.

Gellatly, A.M., and Lyons, T.W., 2005, Trace sulfate in mid-Proterozoic carbonates and the sulfur isotope record of biospheric evolution: Geochimica et Cosmochimica Acta, v. 69, no. 15, p. 3813–3829, doi:10.1016/j.gca.2005.01.019.

Gilleaudeau, G.J., and Kah, L.C., 2015, Heterogeneous redox conditions and a shallow chemocline in the Mesoproterozoic ocean: Evidence from carbon–sulfur–iron relationships: Precambrian Research, v. 257, p. 94–108, doi:10.1016/j.precamres.2014.11.030.

González-Álvarez, I., and Kerrich, R., 2010, REE and HFSE mobility due to protracted flow of basinal brines in the Mesoproterozoic Belt-Purcell Supergroup, Laurentia: Precambrian Research, v. 177, no. 3–4, p. 291–307, doi:10.1016/j.precamres.2009.12.008.

González-Álvarez, I., Kusiak, M.A., and Kerrich, R., 2006, A trace element and chemical Th-U total Pb dating study in the lower Belt-Purcell Supergroup, western North America: Provenance and diagenetic implications: Chemical Geology, v. 230, no. 1–2, p. 140–160, doi:10.1016/j.chemgeo.2005.12.004.

Graham, G., Hitzman, M.W., and Zieg, J., 2012, Geologic setting, sedimentary architecture, and paragenesis of the Mesoproterozoic sediment-hosted Sheep Creek Cu-Co-Ag deposit, Helena Embayment, Montana: Economic Geology and the Bulletin of the Society of Economic Geologists, v. 107, no. 6, p. 1115–1141, doi:10.2113/econgeo.107.6.1115.

Grey, K., and Williams, I.R., 1990, Problematic bedding-plane markings from the Middle Proterozoic Manganese Subgroup, Bangemall Basin, Western Australia: Precambrian Research, v. 46, no. 4, p. 307–327, doi:10.1016/0301-9268(90)90018-L.

Griffith, E.M., and Paytan, A., 2012, Barite in the ocean—Occurrence, geochemistry and palaeoceanographic applications: Sedimentology, v. 59, no. 6, p. 1817–1835, doi:10.1111/j.1365-3091.2012.01327.x.

Hall, A.J., 1986, Pyrite-pyrrhotine redox reactions in nature: Mineralogical Magazine, v. 50, p. 223–229, doi:10.1180/minmag.1986.050.356.05.

Hamilton, J., Bishop, D., Morris, H., and Owens, O., 1982, Geology of the Sullivan orebody, Kimberley, BC, Canada, *in* Hutchison, R.W., Spence, C.D., and Franklin, J.M., eds., Precambrian Sulphide Deposits: Geological Association of Canada Special Paper 25, p. 597–665.

Hanor, J.S., 2000, Barite-celestine geochemistry and environments of formation: Reviews in Mineralogy and Geochemistry, v. 40, no. 1, p. 193–275, doi:10.2138/rmg.2000.40.4.

Harrison, J.E., 1972, Precambrian Belt Basin of northwestern United States: Its geometry, sedimentation, and copper occurrences: Geological Society of America Bulletin, v. 83, no. 5, p. 1215–1240, doi:10.1130/0016-7606(1972)83[1215:PBBONU]2.0.CO;2.

Harrison, J.E., Whipple, J.W., Lidke, D.J., Helen, Z., and Miller, R.J., 1998, Geologic Map of the Western Part of the Cut Bank 1 Degree by 2 Degrees Quadrangle, Northwestern Montana: U.S. Geological Survey Geologic Investigations Series I-2593, scale 1:250,000.

Heslop, D., Dekkers, M., Kruiver, P., and Van Oorschot, I., 2002, Analysis of isothermal remanent magnetization acquisition curves using the expectation-maximization algorithm: Geophysical Journal International, v. 148, no. 1, p. 58–64, doi:10.1046/j.0956-540x.2001.01558.x.

Hoffman, P.F., 1988, Belt Basin: A landlocked remnant oceanic basin? (Analogous to the south Caspian Sea and Black Seas): Geological Society of America Abstracts with Programs, v. 20, p. A40.

Hofmann, H.J., Ediacaran enigmas, and puzzles from earlier times, *in* Proceedings of the Geological Association of Canada–Mineralogical Association of Canada, Joint Annual Meeting, Abstracts 2001: Geological Association of Canada, v. 26, p. 64–65.

Holland, H.D., 1984, The Chemical Evolution of the Atmosphere and Oceans: Princeton, New Jersey, Princeton University Press, 598 p.

Holland, H.D., 2006, The oxygenation of the atmosphere and oceans: Philosophical Transactions of the Royal Society of London, ser. B, Biological Sciences, v. 361, no. 1470, p. 903–915, doi:10.1098/rstb.2006.1838.

Horng, C.-S., and Roberts, A.P., 2006, Authigenic or detrital origin of pyrrhotite in sediments?: Resolving a paleomagnetic conundrum: Earth and Planetary Science Letters, v. 241, no. 3–4, p. 750–762, doi:10.1016/j.epsl.2005.11.008.

Horodyski, R.J., 1982, Problematic bedding-plane markings from the middle Proterozoic Appekunny argillite, Belt Supergroup, northwestern Montana: Journal of Paleontology, v. 56, p. 882–889.

Horodyski, R.J., 1993, Paleontology of Proterozoic shales and mudstones: Examples from the Belt Supergroup, Chuar Group and Pahrump Group, western USA: Precambrian Research, v. 61, no. 3–4, p. 241–278, doi:10.1016/0301-9268(93)90116-J.

Horodyski, R.J., Winston, D., and Whipple, J.W., 1989, Paleontology of the middle Proterozoic Belt Supergroup, *in* Winston, D., Horodyski, R.J., and Whipple, J.W., eds., Middle Proterozoic Belt Supergroup, Western Montana: Great Falls, Montana, to Spokane, Washington: 28th International Geological Congress Field Trip Guidebook T334, p. 7–26.

Hrouda, F., 2003, Indices for numerical characterization of the alteration processes of magnetic minerals taking place during investigation of temperature variation of magnetic susceptibility: Studia Geophysica et Geodaetica, v. 47, no. 4, p. 847–861, doi:10.1023/A:1026398920172.

Huebschman, R.P., 1973, Correlation of fine carbonaceous bands across a Precambrian stagnant basin: Journal of Sedimentary Research, v. 43, no. 3–4, p. 688–699.

Johnson, H.P., Lowrie, W., and Kent, D.V., 1975, Stability of anhysteretic remanent magnetization in fine and coarse magnetite and maghemite particles: Geophysical Journal of the Royal Astronomical Society, v. 41, no. 1, p. 1–10, doi:10.1111/j.1365-246X.1975.tb05480.x.

Johnson, J.E., Gerpheide, A., Lamb, M.P., and Fischer, W.W., 2014, O_2 constraints from Paleoproterozoic detrital pyrite and uraninite: Geological Society of America Bulletin, v. 126, no. 5–6, p. 813–830, doi:10.1130/B30949.1.

Kendall, B., Creaser, R.A., Gordon, G.W., and Anbar, A.D., 2009, Re-Os and Mo isotope systematics of black shales from the Middle Proterozoic Velkerri and Wollogorang formations, McArthur Basin, northern Australia: Geochimica et Cosmochimica Acta, v. 73, no. 9, p. 2534–2558, doi:10.1016/j.gca.2009.02.013.

Kirschvink, J.L., Kopp, R.E., Raub, T.D., Baumgartner, C.T., and Holt, J.W., 2008, Rapid, precise, and high-sensitivity acquisition of paleomagnetic and rock-magnetic data: Development of a low-noise automatic sample changing system for superconducting rock magnetometers: Geochemistry Geophysics Geosystems, v. 9, no. 5, Q05Y01, doi:10.1029/2007GC001856.

Klein, F., Bach, W., Humphris, S.E., Kahl, W.-A., Jöns, N., Moskowitz, B., and Berquó, T.S., 2014, Magnetite in seafloor serpentinite—Some like it hot: Geology, v. 42, no. 2, p. 135–138, doi:10.1130/G35068.1.

Knoll, A.H., Javaux, E.J., Hewitt, D., and Cohen, P., 2006, Eukaryotic organisms in Proterozoic oceans: Philosophical Transactions of the Royal Society of London, ser. B, Biological Sciences, v. 361, no. 1470, p. 1023–1038, doi:10.1098/rstb.2006.1843.

Koski, R.A., and Hein, J.R., 2004, Stratiform Barite Deposits in the Roberts Mountains Allochthon, Nevada: A Review of Potential Analogs in Modern Sea-Floor Environments: U.S. Geological Survey Bulletin 2209-H, 17 p.

Kozłowski, A., Kakol, Z., Kim, D., Zalecki, R., and Honig, J., 1996, Heat capacity of Fe 3-α M α O4 (M = Zn, Ti, $0 \le \alpha \le 0.04$): Physical Review B: Condensed Matter and Materials Physics, v. 54, no. 17, p. 12093.

Larrasoaña, J.C., Roberts, A.P., Musgrave, R.J., Gràcia, E., Piñero, E., Vega, M., and Martínez-Ruiz, F., 2007, Diagenetic formation of greigite and pyrrhotite in gas hydrate marine sedimentary systems: Earth and Planetary Science Letters, v. 261, no. 3–4, p. 350–366, doi:10.1016/j.epsl.2007.06.032.

Li, H.Y., and Zhang, S.H., 2005, Detection of mineralogical changes in pyrite using measurements of temperature-dependence susceptibilities: Chinese Journal of Geophysics, v. 48, no. 6, p. 1454–1461, doi:10.1002/cjg2.794.

Lowrie, W., and Fuller, M., 1971, Alternating field demagnetization characteristics of multidomain thermoremanent magnetization in magnetite: Journal of Geophysical Research, v. 76, no. 26, p. 6339, doi:10.1029/JB076i026p06339.

Luepke, J.J., 1999, Goechemical Trends in Shales of the Belt Supergroup, Northwestern US: A Marine Model for the Evolution of the Mesoproterozoic Western Laurentian Margin [M.S. thesis]: Columbia, Missouri, University Missouri–Columbia, 133 p.

Luepke, J.J., and Lyons, T.W., 2001, Pre-Rodinian (Mesoproterozoic) supercontinental rifting along the western margin of Laurentia: Geochemical evidence from the Belt-Purcell Supergroup: Precambrian Research, v. 111, no. 1, p. 79–90.

Lyons, T.W., and Severmann, S., 2006, A critical look at iron paleoredox proxies: New insights from modern euxinic marine basins: Geochimica et Cosmochimica Acta, v. 70, no. 23, p. 5698–5722, doi:10.1016/j.gca.2006.08.021.

Lyons, T.W., Luepke, J.J., Schreiber, M.E., and Zieg, G.A., 2000, Sulfur geochemical constraints on Mesoproterozoic restricted marine deposition: Lower Belt Supergroup, northwestern United States: Geochimica et Cosmochimica Acta, v. 64, no. 3, p. 427–437, doi:10.1016/S0016-7037(99)00323-3.

Maxwell, D., and Hower, J., 1967, High-grade diagenesis and low-grade metamorphism of illite in Precambrian Belt series: The American Mineralogist, v. 52, no. 5–6, p. 843–857.

Minyuk, P., Subbotnikova, T., and Plyashkevich, A., 2011, Measurements of thermal magnetic susceptibility of hematite and goethite: Izvestiya: Physics of the Solid Earth, v. 47, no. 9, p. 762–774, doi:10.1134/S1069351311080052.

Minyuk, P., Tyukova, E., Subbotnikova, T., Kazansky, A.Y., and Fedotov, A., 2013, Thermal magnetic susceptibility data on natural iron sulfides of northeastern Russia: Russian Geology and Geophysics, v. 54, no. 4, p. 464–474, doi:10.1016/j.rgg.2013.03.008.

Moreau, M., Ader, M., and Enkin, R., 2005, The magnetization of clay-rich rocks in sedimentary basins: Low-temperature experimental formation of magnetic carriers in natural samples: Earth and Planetary Science Letters, v. 230, no. 1–2, p. 193–210, doi:10.1016/j.epsl.2004.11.013.

Moskowitz, B.M., Jackson, M., and Kissel, C., 1998, Low-temperature magnetic behavior of titanomagnetites: Earth and Planetary Science Letters, v. 157, no. 3–4, p. 141–149, doi:10.1016/S0012-821X(98)00033-8.

Mudge, M.R., Erickson, R.L., Kleinkopf, M.D., and Zartman, R.E., 1968, Reconnaissance Geology, Geophysics, and Geochemistry of the Southeastern Part of the Lewis and Clark Range, Montana: U.S. Geological Survey Bulletin 1252-E, p. E1–E35.

O'Day, P.A., Rivera, N., Root, R., and Carroll, S.A., 2004, X-ray absorption spectroscopic study of Fe reference compounds for the analysis of natural sediments: The American Mineralogist, v. 89, no. 4, p. 572–585, doi:10.2138/am-2004-0412.

O'Reilly, W., 1984, Rock and Mineral Magnetism: New York, Chapman and Hall, 220 p., doi:10.1007/978-1-4684-8468-7.

Peters, C., and Dekkers, M., 2003, Selected room temperature magnetic parameters as a function of mineralogy, concentration and grain size: Physics and Chemistry of the Earth, Parts A/B/C, v. 28, no. 16–19, p. 659–667, doi:10.1016/S1474-7065(03)00120-7.

Piatak, N.M., Seal, R.R., Sanzolone, R.F., Lamothe, P.J., Brown, Z., and Adams, M., 2007, Sequential Extraction Results and Mineralogy of Mine Waste and Stream Sediments Associated with Metal Mines in Vermont, Maine, and New Zealand: U.S. Geological Survey Open-File Report 1063, 34 p.

Planavsky, N.J., McGoldrick, P., Scott, C.T., Li, C., Reinhard, C.T., Kelly, A.E., Chu, X., Bekker, A., Love, G.D., and Lyons, T.W., 2011, Widespread iron-rich conditions in the mid-Proterozoic ocean: Nature, v. 477, no. 7365, p. 448–451, doi:10.1038/nature10327.

Potter, D., and Stephenson, A., 1986, The detection of fine particles of magnetite using anhysteretic and rotational remanent magnetizations: Geophysical Journal International, v. 87, no. 2, p. 569–582, doi:10.1111/j.1365-246X.1986.tb06638.x.

Poulton, S.W., and Canfield, D.E., 2011, Ferruginous conditions: A dominant feature of the ocean through Earth's history: Elements (Quebec), v. 7, no. 2, p. 107–112, doi:10.2113/gselements.7.2.107.

Pratt, B.R., 2001, Oceanography, bathymetry and syndepositional tectonics of a Precambrian intracratonic basin: Integrating sediments, storms, earthquakes and tsunamis in the Belt Supergroup (Helena Formation, ca. 1.45 Ga), western North America: Sedimentary Geology, v. 141–142, p. 371–394, doi:10.1016/S0037-0738(01)00083-5.

Price, R., 1964, The Precambrian Purcell System in the Rocky Mountains of southern Alberta and British Columbia: Bulletin of Canadian Petroleum Geology, v. 12, no. 2, p. 399–426.

Raiswell, R., and Canfield, D.E., 1998, Sources of iron for pyrite formation in marine sediments: American Journal of Science, v. 298, no. 3, p. 219–245, doi:10.2475/ajs.298.3.219.

Raub, T., Johnson, S.C., and Raub, T.D., 2012, Rock magnetic detection of the pyrite-to-pyrrhotite reduction: Applications to hydrocarbon maturity, mineral resources, and biogeochemistry: San Francisco, California, American Geophysical Union, Fall Meeting, abstract GP34A-08.

Retallack, G.J., Dunn, K.L., and Saxby, J., 2013, Problematic Mesoproterozoic fossil *Horodyskia* from Glacier National Park, Montana, USA: Precambrian Research, v. 226, p. 125–142, doi:10.1016/j.precamres.2012.12.005.

Robertson, D., and France, D., 1994, Discrimination of remanence-carrying minerals in mixtures, using isothermal remanent magnetisation acquisition curves: Physics of the Earth and Planetary Interiors, v. 82, no. 3–4, p. 223–234, doi:10.1016/0031-9201(94)90074-4.

Ross, C.P., 1959, Geology of Glacier National Park and the Flathead Region, Northwestern Montana: U.S. Geological Survey Professional Paper 296, 125 p., 4 plates.

Ross, G.M., and Villeneuve, M., 2003, Provenance of the Mesoproterozoic (1.45 Ga) Belt Basin (western North America): Another piece in the pre-Rodinia paleogeographic puzzle: Geological Society of America Bulletin, v. 115, no. 10, p. 1191–1217, doi:10.1130/B25209.1.

Schieber, J., 1989, Pyrite mineralization in microbial mats from the mid-Proterozoic Newland Formation, Belt Supergroup, Montana, USA: Sedimentary Geology, v. 64, no. 1–3, p. 79–90, doi:10.1016/0037-0738(89)90085-7.

Sears, J., Chamberlain, K., and Buckley, S., 1998, Structural and U-Pb geochronological evidence for 1.47 Ga rifting in the Belt Basin, western Montana: Canadian Journal of Earth Sciences, v. 35, no. 4, p. 467–475, doi:10.1139/e97-121.

Shannon, R.D., and White, J.R., 1991, The selectivity of a sequential extraction procedure for the determination of iron oxyhydroxides and iron sulfides in lake sediments: Biogeochemistry, v. 14, no. 3, p. 193–208, doi:10.1007/BF00000807.

Shen, Y., Knoll, A.H., and Walter, M.R., 2003, Evidence for low sulphate and anoxia in a mid-Proterozoic marine basin: Nature, v. 423, no. 6940, p. 632–635, doi:10.1038/nature01651.

Skomurski, F.N., Kerisit, S., and Rosso, K.M., 2010, Structure, charge distribution, and electron hopping dynamics in magnetite (Fe_3O_4) (100) surfaces from first principles: Geochimica et Cosmochimica Acta, v. 74, no. 15, p. 4234–4248, doi:10.1016/j.gca.2010.04.063.

Slack, J., Grenne, T., Bekker, A., Rouxel, O., and Lindberg, P., 2007, Suboxic deep seawater in the late Paleoproterozoic: Evidence from hematitic chert and iron formation related to seafloor-hydrothermal sulfide deposits, central Arizona, USA: Earth and Planetary Science Letters, v. 255, no. 1–2, p. 243–256, doi:10.1016/j.epsl.2006.12.018.

Slotznick, S.P., Zieg, J., Webb, S.M., Kirschvink, J.L., and Fischer, W.W., 2015, Iron mineralogy and redox chemistry of the Mesoproterozoic Newland Formation in the Helena Embayment, Belt Supergroup, Montana: Northwest Geology, v. 44, p. 55–72.

Snowball, I.F., 1997, The detection of single-domain greigite (Fe_3S_4) using rotational remanent magnetization (RRM) and the effective gyro field (Bg): Mineral magnetic and palaeomagnetic applications: Geophysical Journal International, v. 130, no. 3, p. 704–716, doi:10.1111/j.1365-246X.1997.tb01865.x.

Sperling, E., Rooney, A., Hays, L., Sergeev, V., Vorob'eva, N., Sergeeva, N., Selby, D., Johnston, D., and Knoll, A., 2014, Redox heterogeneity of subsurface waters in the Mesoproterozoic ocean: Geobiology, v. 12, no. 5, p. 373–386, doi:10.1111/gbi.12091.

Sperling, E.A., Wolock, C.J., Morgan, A.S., Gill, B.C., Kunzmann, M., Halverson, G.P., Macdonald, F.A., Knoll, A.H., and Johnston, D.T., 2015, Statistical analysis of iron geochemical data suggests limited late Proterozoic oxygenation: Nature, v. 523, no. 7561, p. 451–454, doi:10.1038/nature14589.

Stanley, A., and Davies-Vollum, K., 2000, A Detailed Sedimentary Analysis of the Middle Part of the Grinnell Formation, near Going-to-the-Sun Mountain, Glacier National Park, Montana: National Park Service Investigator's Annual Report 19879, 2 p.

Stewart, J.H., 1972, Initial deposits in the Cordilleran geosyncline: Evidence of a late Precambrian (<850 my) continental separation: Geological Society of America Bulletin, v. 83, no. 5, p. 1345–1360, doi:10.1130/0016-7606(1972)83[1345:IDITCG]2.0.CO;2.

Stüeken, E.E., 2013, A test of the nitrogen-limitation hypothesis for retarded eukaryote radiation: Nitrogen isotopes across a Mesoproterozoic basinal profile: Geochimica et Cosmochimica Acta, v. 120, p. 121–139, doi:10.1016/j.gca.2013.06.002.

Suzuki, Y., Kopp, R.E., Kogure, T., Suga, A., Takai, K., Tsuchida, S., Ozaki, N., Endo, K., Hashimoto, J., and Kato, Y., 2006, Sclerite formation in the hydrothermal-vent "scaly-foot" gastropod—Possible control of iron sulfide biomineralization by the animal: Earth and Planetary Science Letters, v. 242, no. 1–2, p. 39–50, doi:10.1016/j.epsl.2005.11.029.

Thomson, G.F., 1990, The anomalous demagnetization of pyrrhotite: Geophysical Journal International, v. 103, no. 2, p. 425–430, doi:10.1111/j.1365-246X.1990.tb01781.x.

Vitorello, I., and Van der Voo, R., 1977, Late Hadrynian and Helikian pole positions from the Spokane formation, Montana: Canadian Journal of Earth Sciences, v. 14, no. 1, p. 67–73, doi:10.1139/e77-007.

Walcott, C.D., 1899, Pre-Cambrian fossiliferous formations: Geological Society of America Bulletin, v. 10, no. 1, p. 199–244, doi:10.1130/GSAB-10-199.

Walter, M., Oehler, J.H., and Oehler, D.Z., 1976, Megascopic algae 1300 million years old from the Belt Supergroup, Montana: A reinterpretation of Walcott's Helminthoidichnites: Journal of Paleontology, v. 50, p. 872–881.

Walter, M., Rulin, D., and Horodyski, R.J., 1990, Coiled carbonaceous megafossils from the Middle Proterozoic of Jixian (Tianjin) and Montana: American Journal of Science, v. 290, p. 133–148.

Weaver, R., Roberts, A.P., and Barker, A.J., 2002, A late diagenetic (syn-folding) magnetization carried by pyrrhotite: Implications for paleomagnetic studies from magnetic iron sulphide-bearing sediments: Earth and Planetary Science Letters, v. 200, no. 3–4, p. 371–386, doi:10.1016/S0012-821X(02)00652-0.

Webb, S.M., 2005, SIXPACK: A graphical user interface to XAS analysis using IFEFFIT: Physica Scripta, v. T115, p. 1011–1014, doi:10.1238/Physica.Topical.115a01011.

Webb, S.M., 2011, The MicroAnalysis Toolkit: X-ray fluorescence image processing software: American Institute of Physics (AIP) Conference Proceedings, v. 1365, p. 196–199, doi:10.1063/1.3625338.

Whipple, J., Binda, P., and Winston, D., 1997, Geologic guide to Glacier National Park, Montana, and areas adjacent to Waterton, Alberta., *in* Proceedings of the Belt Symposium III: Geologic Guidebook to the Belt-Purcell Supergroup, Glacier National Park and Vicinity, Montana and Adjacent Canada: Pocatello, Idaho, Belt Association, p. 125–155.

Whipple, J.W., Connor, J.J., Raup, O.B., and McGimsey, R.G., 1984, Preliminary report on the stratigraphy of the Belt Supergroup, Glacier National Park and adjacent Whitefish Range, Montana, *in* McBane, J.D., and Garrison, P.B., eds., Guidebook for the Field Conference and Symposium, Belt Association: Pocatello, Idaho, Montana Geological Society, p. 33–50.

Whipple, J.W., Donatich, A.J., and Williams, H.F., 1992, Geologic Map of Glacier National Park, Montana: U.S. Geological Survey Miscellaneous Investigations Series Map I-1508-F, scale 1:100,000.

Wilkin, R., Barnes, H., and Brantley, S., 1996, The size distribution of framboidal pyrite in modern sediments: An indicator of redox conditions: Geochimica et Cosmochimica Acta, v. 60, no. 20, p. 3897–3912, doi:10.1016/0016-7037(96)00209-8.

Willis, B., 1902, Stratigraphy and structure, Lewis and Livingston ranges, Montana: Geological Society of America Bulletin, v. 13, no. 1, p. 305–352, doi:10.1130/GSAB-13-305.

Winston, D., 1986a, Belt Supergroup Stratigraphic Correlation Sections, Western Montana and Adjacent Areas: Montana Bureau of Mines and Geology Geologic Map 40, 16 p., 1 sheet.

Winston, D., 1986b, Sedimentation and tectonics of the middle Proterozoic Belt Basin and their influence on Phanerozoic compression and extension in western Montana and northern Idaho: Part II. Northern Rocky Mountains, *in* Peterson, J.A., ed., Paleotectonics and Sedimentation in the Rocky Mountain Region, United States: American Association of Petroleum Geologists Memoir 41, p. 87–118.

Winston, D., 1986c, Sedimentology of the Ravalli Group, middle Belt carbonate, and Missoula Group, Middle Proterozoic Belt Supergroup, Montana, Idaho, and Washington, *in* Roberts, S.M., ed., Belt Supergroup: A Guide to Proterozoic Rocks of Western Montana and Adjacent Areas: Montana Bureau of Mines and Geology Special Publication 94, p. 85–124.

Winston, D., 2007, Revised Stratigraphy and Depositional History of the Helena and Wallace Formations, Mid-Proterozoic Piegan Group: Belt Supergroup Montana and Idaho, *in* Link, P.K., and Lewis R.S., eds., Proterozoic Geology of Western North America and Siberia: Society for Sedimentary Geology (SEPM) Special Publication 86, p. 65–100.

Winston, D., 2016, this volume, Sheetflood sedimentology of the Middle Proterozoic Revett Formation, Belt Supergroup, Montana, USA, *in* MacLean, J.S., and Sears, J.W., eds., Belt Basin: Window to Mesoproterozoic Earth: Geological Society of America Special Paper 522, doi:10.1130/2016.2522(01).

Winston, D., and Link, P., 1993, Middle Proterozoic rocks of Montana, Idaho, and eastern Washington: The Belt Supergroup, *in* Reed, J.C., Jr., et al., eds., Precambrian: Conterminous U.S.: Boulder, Colorado, Geological Society of America, Geology of North America, v. 2, p. 487–517.

Xu, S., and Dunlop, D. J., 1995, Toward a better understanding of the Lowrie-Fuller test: Journal of Geophysical Research–Solid Earth (1978–2012), v. 100, no. B11, p. 22,533–22,542.

Zhang, C., Paterson, G.A., and Liu, Q., 2012, A new mechanism for the magnetic enhancement of hematite during heating: The role of clay minerals: Studia Geophysica et Geodaetica, v. 56, no. 3, p. 845–860, doi:10.1007/s11200-011-9018-4.

Zhou, T., Phillips, G.N., Dong, G., and Myers, R.E., 1995, Pyrrhotite in the Witwatersrand gold fields, South Africa: Economic Geology and the Bulletin of the Society of Economic Geologists, v. 90, no. 8, p. 2361–2369, doi:10.2113/gsecongeo.90.8.2361.

Manuscript Accepted by the Society 10 December 2015
Manuscript Published Online 16 March 2016